UNIVERSIDADE FEDERAL DE MINAS GERAIS
Escola de Engenharia
Programa de Pós-Graduação em Engenharia Metalúrgica, Materiais e de Minas

Olavo Carvalho Haase

Fabricação de uma Liga de Al-4%Cu de Alta Resistência Mecânica via Consolidação de Partículas por Torção sob Alta Pressão

Belo Horizonte

2023

Olavo Carvalho Haase

Fabricação de uma Liga de Al-4%Cu de Alta Resistência Mecânica via Consolidação de Partículas por Torção sob Alta Pressão

Dissertação apresentada ao Programa de Pós-Graduação em Engenharia Metalúrgica, Materiais e de Minas da Escola de Engenharia da Universidade Federal de Minas Gerais como requerimento para obtenção do grau de Mestre em Engenharia Metalúrgica, Materiais e de Minas.

Área de concentração: Metalurgia Física e de Transformação.

Orientador: Prof. Pedro Henrique Rodrigues Pereira.

Belo Horizonte
2023

Haase, Olavo Carvalho.
H112f Fabricação de uma liga de Al-4%Cu de alta resistência mecânica via consolidação de partículas por torção sob alta pressão [recurso eletrônico] / Olavo Carvalho Haase. – 2023.
1 recurso online (90 f. : il., color.) : pdf.

Orientador: Pedro Henrique Rodrigues Pereira.

Dissertação (mestrado) – Universidade Federal de Minas Gerais, Escola de Engenharia.

Bibliografia: f. 77-90.
Exigências do sistema: Adobe Acrobat Reader.

1. Engenharia metalúrgica – Teses. 2. Metalurgia física – Teses. 3. Metais – Propriedades mecânicas – Teses. 4. Precipitação (Química) – Teses. 5. Pressão alta (Tecnologia) – Teses. 6. Ligas de cobre – Teses. 7. Ligas de alumínio – Teses. I. Pereira, Pedro Henrique Rodrigues. II. Universidade Federal de Minas Gerais. Escola de Engenharia. III. Título.

CDU: 669(043)

Ficha catalográfica elaborada pelo Bibliotecário Marcio Anderson de Andrade Gomes CRB/6 2812
Biblioteca Prof. Mário Werneck, Escola de Engenharia da UFMG

Folha de aprovação

UNIVERSIDADE FEDERAL DE MINAS GERAIS
ESCOLA DE ENGENHARIA
Programa de Pós-Graduação em Engenharia Metalúrgica, Materiais e de Minas

A dissertação intitulada **"Fabrication of a High-Strength Al-Cu Alloy through Cold Consolidation of Powders using High-Pressure Torsion"**, área de concentração: Metalurgia Física e de Transformação, apresentada pelo candidato **Olavo Carvalho Haase**, para obtenção do grau de Mestre em Engenharia Metalúrgica, Materiais e de Minas, foi aprovada pela comissão examinadora constituída pelos seguintes membros:

Dr. Pedro Henrique Rodrigues Pereira
Orientador (UFMG)

Dra. Augusta Cerceau Isaac Neta
(UFMG)

Dr. Wellington Lopes
(CEFET/MG)

Dr. Paulo Roberto Cetlin
(UFMG)

Coordenador do Programa de Pós-Graduação em Engenharia Metalúrgica, Materiais e de Minas/UFMG

Belo Horizonte, 24 de maio de 2023

UNIVERSIDADE FEDERAL DE MINAS GERAIS
Escola de Engenharia
Programa de Pós-Graduação em Engenharia Metalúrgica, Materiais e de Minas

Olavo Carvalho Haase

Fabrication of a high-strength Al-Cu alloy through cold-consolidation of powders using high-pressure torsion

Belo Horizonte

2023

Olavo Carvalho Haase

Fabrication of a high-strength Al-Cu alloy through cold-consolidation of powders using high-pressure torsion

Master's degree dissertation presented to the Graduate Program of Metallurgical, Materials and Mining Engineering of the Federal University of Minas Gerais, as a partial requirement to the master's degree in metallurgical, Materials and Mining Engineering.

Research area: Physical Metallurgy

Advisor: Dr. Pedro Henrique Rodrigues Pereira

Belo Horizonte
2023

Acknowledgements

The author is grateful to everyone who participated in the development of this research work and, in particular:

- My advisor Dr. Pedro Henrique Rodrigues Pereira for the counseling and insightful guidance provided constantly;
- All professors who generously assisted me throughout my academic trajectory and the development of this work with essential teachings, as well as, by allowing the usage of the structure of laboratories and equipments. Namelly, Dr. Paulo Roberto Cetlin, Dr. Alisson Duarte da Silva, Dr. Roberto Braga Figueiredo, Dr. Dagoberto Brandão Santos, Dr. Witor Wolf, Dr. Maurício Bagatini, Dr. Vicente Buono and Dr. Berenice Gonzales;
- The technicians Tiago Elias, Samuel, Leonardo and Patrícia that greatly helped in the processing and examination of the Al-Cu samples;
- The members of the secretariats Maria Aparecida Pacheco, Diego Soares and Kelly Bretz;
- All the colleagues that contributed with operational instructions or pleasant daily camaraderie, in special: Pedro Henrique Silva, Adriano Trajano, Davi Alves, Guilherme Cardeal Stumpf, Raphael França, Amanda Carvalho, Leonardo Mayer, Natanael Almeida, Nayara Azevedo, Paula Cibely, Denise Machado, Igor Cuzzuol, Lorena Isabela, Lucas Figueiredo and Laís Bonoto;
- The company Altom Metalurgia Ltda. and Walmer Avelar, for the generous donation of the aluminium powder used on the research;
- My family and friends for all the love and support;
- CAPES, CNPq, FAPEMIG, UFMG and PPGEM.

Resumo

A fabricação de nanocompósitos com matriz metálica (MMNC) por meio de consolidação a frio por Deformação Plástica Severa (SPD) destaca-se como uma nova rota de síntese de materiais a partir de partículas metálicas. Esses processos são de interesse acadêmico e industrial por sua aplicabilidade em reciclagem, e no projeto de novos materiais ou microestruturas com propriedades mecânicas e funcionais avançadas, devido à ocorrência de intenso refino de grão, supersaturação de elementos químicos em solução sólida e eventual segregação nos contornos de grão, além da formação de nanoprecipitados. No entanto, estudos adicionais ainda são necessários para melhor entender esses processos e como empregá-los no projeto de propriedades. Portanto, o presente estudo objetivou examinar a evolução microestrutural, nanoestrutural e de propriedades mecânicas de uma liga Al-4%Cu (% em massa) submetida à torção em alta pressão (HPT) por 0,1, 1, 3, 10, 30, 60 e 100 voltas. A liga Al-Cu foi escolhida por seu comportamento conhecido de precipitação, sua reciclabilidade, ampla disponibilidade, baixa densidade e atuação em aplicações estruturais. Diversas análises após o HPT foram conduzidas, incluindo microdureza Vickers, microscopia eletrônica de varredura, difração de raios-X, microscopia eletrônica de transmissão, espectroscopia de raios-X por dispersão em energia e ensaios de compressão no estado plano de deformação. Os resultados demonstraram que o HPT promoveu a plena consolidação das partículas de cobre e alumínio, de modo que a liga Al-4Cu alcançou elevada dureza (~270 Hv) e grãos nanométricos (~48 nm) após processamento por 100 voltas. Inicialmente as partículas se esticaram, o que levou à instabilidades de fluxo e à formação de estruturas do tipo vórtice e, finalmente, ocorreu a fragmentação das partículas e a solubilização sólida parcial do cobre na matriz de alumínio.

Palavras-chave: Liga de alumínio; Consolidação de Partículas; Precipitação dinâmica; Refino de grão; Torção sob Alta Pressão.

Abstract

The fabrication Metal-Matrix Nanocomposites (MMNC) and alloys through cold-consolidation by Severe Plastic Deformation (SPD) is a novel possibility that requires further investigation. These processes are of interest as consequence of their applicability in recycling and in tailoring new materials or microstructures with enhanced mechanical and functional properties due to the occurrence of internal processes, such as intensive grain refinement, grain boundary segregation, formation of nano-precipitates or solubilization of precipitates. Further studies are necessary to better understand these processes and how to employ them in the tailoring of mechanical and functional material properties. Therefore, this study aimed to examine the microstructural and mechanical properties evolution of an Al-Cu alloy subjected to High Pressure Torsion at 1, 3, 10, 30, 60, and 100 turns. The Al-Cu alloy was chosen because of its known precipitation behaviour, recyclability, wide availability, low density, and employment in structural applications. Several analyses were conducted on the samples after HPT, namely Vickers microhardness tests, Scanning Electron Microscopy (SEM), X-Ray Diffraction (XRD), Transmission Electron Microscopy (TEM), Energy-Dispersive X-ray Spectroscopy (EDS), Selected Area Electron Diffraction (SAED) and Ford Compression Test. The results demonstrate that consolidation was achieved after 30 turns, furthermore, enhanced strength properties (~270 Hv hardness) and small grain sizes (~48 nm) were obtained and behavior of the Cu particles under strain was described. Initially the particles stretched, which then led to flow instabilities and the formation of vortice-like structures, and finally, the particles fragmented and solid solubilization of the Cu on the Al matrix occurred.

Keywords: Aluminium alloy; Consolidation of powders; Dynamic precipitation; Grain refinement; High-pressure torsion.

List of Figures

List of Tables

Definitions and Abbreviations

ARB – Accumulative Roll Bonding

at% - Atomic Percent

BCC – Body-Centred Cubic

BSE - Back Scattered Electrons

CG – Coarse-Grained

ECAE – Equal Channel Angular Extrusion

ECAP – Equal Channel Angular Pressing

EDS - Energy-Dispersive X-ray Spectroscopy

FCC – Face-Centred Cubic

FEM – Finite Elements Method

FIB – Focused Ion Beam

GP – Guinier Preston

GPa – Giga Pascal

HAGB – High-Angle Grain Boundary

Hv – Hardness Vickers

HPT – High Pressure Torsion

MAUD - Material Analyses Using Diffraction

MDF – Multi-Directional Forging

MDCF - Multi-Directional Confined Forging

MEMS – Microelectromechanical Systems

mm - Milimeter

MMNC – Metal-Matrix Nanocomposites

PSC – Plane Strain Compression

rpm – Rotation per Minute

SAED – Selected Area Electron Diffraction

SE – Secondary Electrons

SEM – Scanning Electron Microscopy

SPD – Severe Plastic Deformation

STEM - Scanning Transmission Electron Microscopy

TE – Twist Extrusion

TEM – Transmission Electron Microscopy

UFG – Ultrafine-Grained

XRD – X-Ray Diffraction

wt% - Weight Percent

n – Number of turns

r – Distance from centre

t – Thickness of the sample

α – Aluminium phase in the Al rich Al-Cu system

ε – Strain

μm -Micrometer

θ – Al_2Cu intermetallic

Table of Contents

1 Introdução

O desenvolvimento de ligas metálicas com maior relação entre resistência mecânica e peso específico é de fundamental importância para a indústria de transportes, que demanda a redução das emissões de CO_2. A exemplo da indústria automotiva, peças compostas por materiais com maior resistência mecânica e menos densos que o aço, como o alumínio e o cobre, se traduziriam em componentes mais leves e, portanto, em veículos com eficiência energética superior. No quesito sustentabilidade, o alumínio é um material com alto potencial de reciclagem e é possível fabricar compósitos de matriz de Al por meio da reciclagem de sucatas e outros particulados em estado sólido, mesmo em temperatura ambiente, por meio de procedimentos de Deformação Plástica Severa (SPD), como Torção sob Alta Pressão (HPT) (WAN et al., 2017).

Além disso, a consolidação usando HPT permite o aumento da resistência mecânica do material por diferentes mecanismos de endurecimento, como endurecimento por precipitação e refinamento de grão. Esses efeitos podem ser extremamente severos com o HPT, pois é o processo de SPD desenvolvido até então que pode impor as maiores deformações sem trincas no material (ASGHARZADEH; JOO; KIM, 2014; ASHIDA et al., 2012; BRUDER, 2019; EDALATI; HORITA, 2016; KULAGIN et al., 2017, 2018; PATIL et al., 2013). Além disso, o processo de consolidação e SPD pode ser usado para projetar muitas propriedades interessantes para novos materiais (HORITA; EDALATI, 2020), como melhor resistência ao desgaste usando reforços na consolidação (EDALATI et al., 2014), melhor estabilidade térmica, assegurada por segregações nos contornos de grãos que impedem o crescimento do grão (MOHAMMADI et al., 2021; SAUVAGE; DUCHAUSSOY; ZAHER, 2019; SILVA et al., 2020), hidrólise rápida e geração de hidrogênio (ZHANG et al., 2017).

Uma aplicação recente que vem recebendo atenção é o desenvolvimento de ligas reforçadas e nanocompósitos de matriz metálica (MMNC). Esses reforços

podem ser incorporados ao substrato da matriz por consolidação, o que resulta em tamanho de grão final reduzido, devido à ocorrência de segregação no contorno de grão, nanoprecipitados e solubilização (ZHILYAEV et al., 2007). Esta aplicação permite o projeto de ligas com propriedades otimizadas, uma vez que foi demonstrado que as reações podem ser projetadas para alcançar a distribuição microestrutural desejada (SILVA et al., 2020). Outra possibilidade é dissolver precipitados usando SPD e depois reprecipitar para originar precipitados finos e dispersos nos contornos de grão. Dissolução e reprecipitação já foram alcançadas em uma liga Al-1.7at%Cu (MURAYAMA; HORITA; HONO, 2001).

Em resumo, a liga Al-Cu é especialmente interessante para estudar o processo de SPD por causa da solubilidade limitada de Cu em Al à temperatura ambiente, a diferença de resistência mecânica entre as fases e o comportamento de precipitação característico dessa liga, o que sugere que segregação nos contornos de grão, nanoprecipitados ou solubilização podem ocorrer em tensões intensas. Além disso, Al e Cu são materiais com ampla disponibilidade e reciclabilidade.

1.1 Introduction

The development of metallic alloys having a higher strength to specific weight ratio is of crucial importance to the transportation industry, which demands the reduction of CO_2 emissions. Considering the example of the automotive industry, parts composed by materials with higher strength and less dense than steel, such as aluminium and copper, would translate into lighter components and, therefore, vehicles with superior energy efficiency. Regarding sustainability, aluminium emerges as a material with a high recycling potential and it is possible to fabricate load-bearing Al-matrix composites through recycling of scraps and other solid-state particulates, even at room temperature, by Severe Plastic Deformation (SPD) procedures, such as High-Pressure Torsion (HPT) (WAN et al., 2017).

In addition, consolidation using HPT allows the increase of the material strength by different hardening mechanisms, such as precipitate hardening and grain refinement. These effects can be extremely severe with HPT, since it is the SPD process developed so far that can impose the largest deformations without material cracking (ASGHARZADEH; JOO; KIM, 2014; ASHIDA et al., 2012; BRUDER, 2019; EDALATI; HORITA, 2016; KULAGIN et al., 2017, 2018; PATIL et al., 2013). Moreover, the process of consolidation and further SPD can be used to tailor many different interesting properties for novel materials (HORITA; EDALATI, 2020), such as better wear resistance using reinforcements on the consolidation (EDALATI et al., 2014), better thermal stability, assured by segregations on the grain boundaries that hinder grain growth (MOHAMMADI et al., 2021; SAUVAGE; DUCHAUSSOY; ZAHER, 2019; SILVA et al., 2020), fast hydrolysis and hydrogen generation (ZHANG et al., 2017).

A recent application that has been receiving some attention is the development of reinforced alloys and Metal-Matrix Nanocomposites (MMNC). These reinforcements can be incorporated to the matrix substrate and then be subjected to consolidation, which results in reduced final grain size, due to the occurrence

of grain boundary segregation, nanoprecipitates, and solubilization (ZHILYAEV et al., 2007). This application allows for the tailoring of properties, since it has been demonstrated that reactions can be designed to achieve desired microstructural distribution, with enhanced properties and reduced grain size (SILVA et al., 2020). Another possibility is dissolving precipitates using SPD and then reprecipitating to originate fine, disperse equiaxial precipitates on the grain boundaries. Dissolution and reprecipitation has been achieved in an Al-1.7at%Cu alloy (MURAYAMA; HORITA; HONO, 2001).

In summary, the Al-Cu alloy is especially interesting to study the consolidation process because of the limited solubility of Cu in Al at room temperature, the strength difference between the phases, and the characteristic precipitation behavior of the alloy, which suggest that grain boundary segregation, nanoprecipitates or solubilization might occur at intense strains. Furthermore, Al and Cu are materials with wide availability and recyclability.

2 Aim and Objectives

This research aims to study the capabilities of HPT processing as a tool for cold-consolidation of metallic powders composed by Al and Cu and carefully examine the influence of number of turns in the mechanical behavior and microstructural evolution of the HPT-processed alloy. Its novelty, compared to other studies in the literature, rely on carrying out HPT processing up to 100 turns to trigger solid-state reactions, that may lead to further enhancement of the material strength and adequate thermal stability, due to the formation of ultrafine grains accompanied by segregation and fragmentation of nano-sized particles after sufficient torsional straining.

The specific objectives are outlined as follows:

- To identify the different hardening stages achieved and the mixing mechanisms that occurred and the underlying micro/nanostructural evolution in the Al-Cu alloy during HPT processing;
- To assess the consolidation of Al-Cu powders by micrographic analyses and mechanical testing in material processed up to different numbers of turns.

3 Literature Review

3.1 The Al-Cu System

At room temperature, both Aluminium and Copper manifest Face Centred Cubic (FCC) microstructures and form a substitutional solid solution. However, Cu solubility in Al (α phase) at room temperature is very low, leading to the formation of an intermetallic phase at equilibrium, called the θ phase (Al_2Cu). The θ solvus line in the α phase in the Al-Cu phase diagram has an interesting behaviour, in which its solubility increases with temperature, reaching a maximum solubility of approximately 4.5wt% at 548°C. This behaviour is precisely what makes Al-Cu a precipitation hardenable alloy. The Al rich end of the Al-Cu diagram is shown in Figure 1 (ABBASCHIAN; ABBASCHIAN; REED-HILL, 2009; MASSALSKI, 1980).

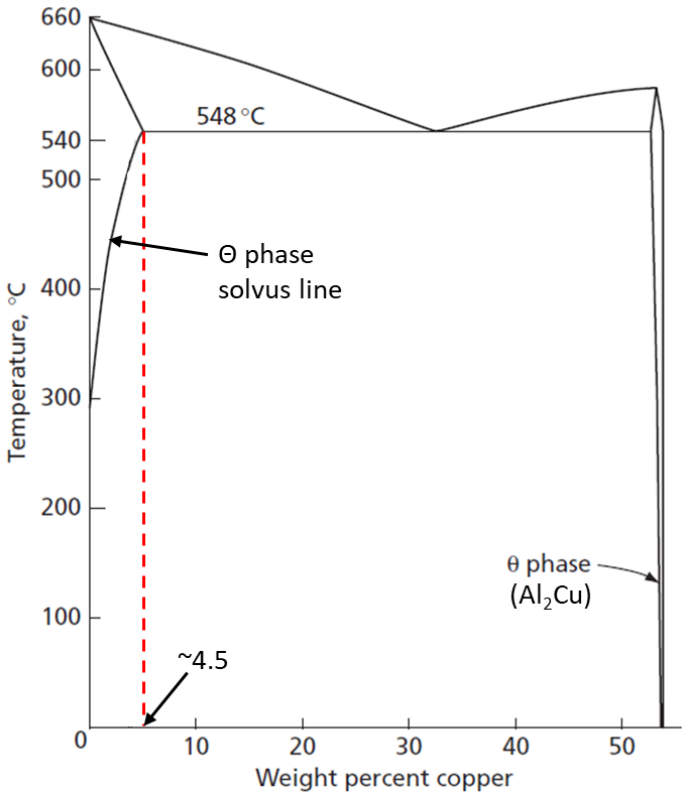

Figure 1: Al rich end of the Al-Cu diagram

(Adapted from ABBASCHIAN; ABBASCHIAN; REED-HILL, 2009)

The Al-Cu alloy has somewhat of a historical relevance regarding the study of age hardening. The first recognition of the increase in strength by the process of ageing happened accidentally in 1906 with an Al-Cu alloy with a small addition of Magnesium, the results were published in 1911 and it was only later, in 1920, that the cause of this increase in strength was associated with the occurrence of precipitation (HORNBOGEN, 2001; I J POLMEAR, 2004; MERICA, 1920; WILM, 1906, 1911). The formation of precipitate in the Al-Cu alloy during an ageing process, follows a sequence dependent on the temperature. Considering a path of increasing temperature, the sequence goes from a supersaturated solid solution of α phase to a saturated solid solution of α phase, going through the formation of incoherent Guinier Preston (GP) zones, followed by semi-coherent θ'' and θ' phases, and finally the coherent θ phase. Maximum yield strength is achieved for Al-Cu precipitation hardened alloys aged at 149°C for approximately 48 hours. This treatment produces fine disperse semi-coherent precipitates and favours heterogeneous precipitation. The precipitation sequence in Al-Cu alloys is shown in Figure 2 (ABBASCHIAN; ABBASCHIAN; REED-HILL, 2009).

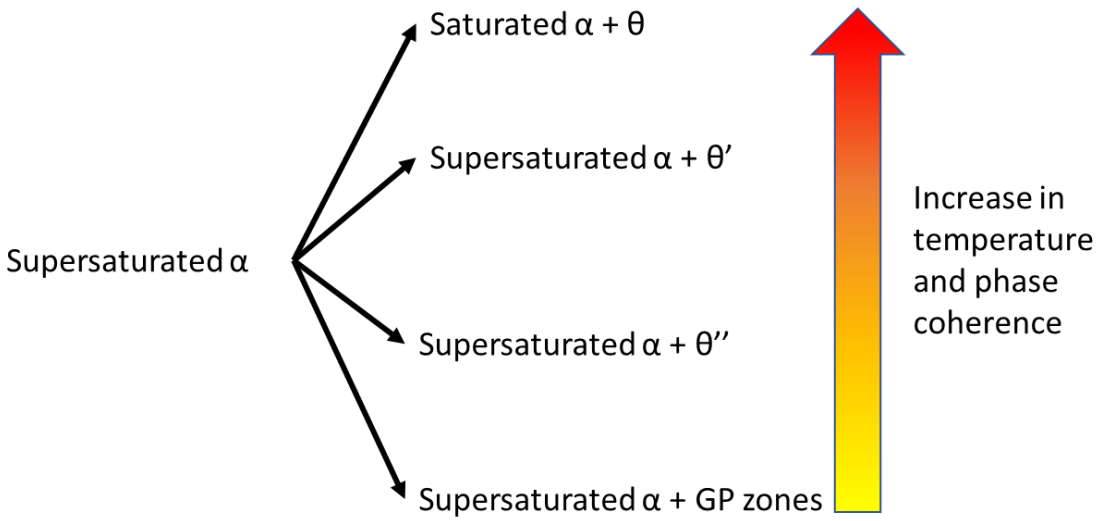

Figure 2: Precipitation sequence in the Al-Cu alloy
(Adapted from ABBASCHIAN; ABBASCHIAN; REED-HILL, 2009).

Early studies on the dissolution and formation behaviour of precipitates in the Al-Cu alloy revealed several interesting findings. For instance, the dissolution of Widmanstatten particles of θ phase occurs by diffusion of Cu in the Al matrix (HALL; HAWORTHJ, 1970), the confirmation of the precipitation sequence and the anomalous coarsening behaviour of the θ’ phase (initially faster than predicted by theory of the time, followed by a sharp decrease in the coarsening rate) (BOYD; NICHOLSON, 1971). An in-situ study described the kinetic of transition from the θ’ to the stable θ phase through nucleation and growth of the θ phase in the α/θ’ interface (LAIRDT; AARONSON, 1966) and another in-situ study revealed that the dissolution rate of θ’ phase decreases with an increase of previously applied deformation. However, at very high strains, the dissolution rate was substantially accelerated, which was explained by excessive vacancies introduced by deformation (HEWITT; BUTLER, 1986). Application of stress during the ageing process has been shown to propitiate the formation of oriented GP zones and θ’ precipitates in an Al-Cu alloy (ETO; SAT0; MORF, 1978). A recent study confirms the precipitation sequence and states that the coarsening of the θ’ phase is in accordance with Liftshitz-Slyozov-Wagner theory (CHEN; ZHAO; ZHANG, 2021).

3.2 Severe Plastic Deformation - SPD

Severe Plastic Deformation (SPD) can be defined as material processing techniques in which large plastic strains are imposed in bulk samples without substantial dimensional changes. The first SPD technique was High-Pressure Torsion (HPT), introduced in 1935. It was characterized by high shear stresses and hydrostatic pressures, which permitted virtually unlimited straining (BRIDGMAN, 1935, 1937). The initial approach to SPD focused solely on grain refinement, which was studied using X-Ray Diffraction (the only method available at the time to study such small grains). Afterwards, Transmission Electron Microscopy (TEM) was applied and permitted the description of the fine grain

microstructures after processing (BRIDGMAN, 1937; NUTTING, 1971; SEGAL, 2018).

The next SPD technique invented was the Equal-Channel Angular Pressing (ECAP), which had the advantage of being able to produce larger billets (SEGAL, 2018, 1974). More recently, new SPD techniques have been introduced, with different advantages and disadvantages, such as Twist-Extrusion (TE), ECAP variations, and SPD by ordinary forming operations, such as Multi-Directional Forging (MDF) and Accumulative Roll Bonding (ARB) (BEYGELZIMER; ORLOV; VARYUKHIN', 2002; IMAYEV; IMAYEV; SALISHCHEV, 1992; KOCICH; KUNICKÁ; MACHÁKOVÁ, 2014; NISHIDA et al., 2001; SAITO et al., 1998; SEGAL, 2018). One of the driving forces responsible for the introduction of new SPD techniques was the necessity of industrial application. Thus, new methods were developed: 1) the semi-continuous SPD operations, such as ECAP, capable of producing large-scale products; and, 2) continuous processes, such as ARB, capable of producing unlimited length products due to the continuous processes having two stress-free ends (EDALATI et al., 2022).

The main hardening mechanism involved in SPD techniques is the increase in the material strength resulting from the decrease in grain size. This behavior may be predicted using the Hall-Petch relation as follows:

$$\sigma_y = \sigma_0 + k_y d^{-0.5} \quad (1)$$

where σ_y is the yield strength, d is the grain size, and σ_0 and k_y are material constants (HALL, 1951; PETCH, 1953). The increase in strength associated with the decrease in grain size occurs for most metals, but this can be inverse in materials subjected to room temperature creep mechanisms such as grain boundary sliding (CASTRO et al., 2020). The strengthening behavior can even be dependent on the strain itself; for instance, early reports stated that aluminum experienced strengthening in early stages of straining followed by softening at large strains (EDALATI et al., 2022). Furthermore, other effects can result in higher mechanical strength than expected by the Hall-Petch relation, *e.g.,* when dislocations are hindered in grain boundaries having a high concentration of

solutes. This behavior is exemplified in Figure 3, where the Hall-Petch relation is confirmed for different Al alloys (VALIEV et al., 2010).

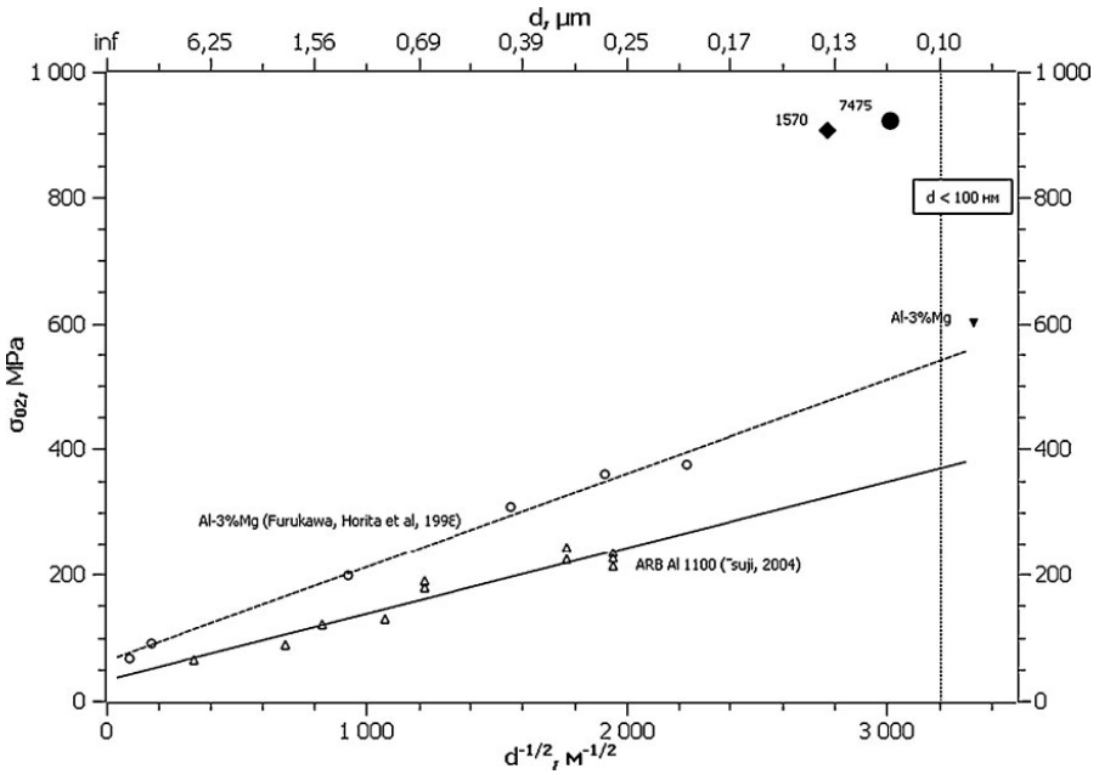

Figure 3:The Hall–Petch relation for the alloys: Al 1100, Al-3%Mg, and data on the YS of the UFG alloys 1570 and 7475
(VALIEV; LANGDON, 2010).

On regular forming operations, grain refinement occurs due to recrystallization, that can be by dynamic or static recrystallization during subsequent annealing. However, grain refinement is observed after cold SPD processing without subsequent annealing, which is currently explained by mechanisms like dynamic recrystallization occurring at large strains which lead to the formation of high-angle grain boundaries (HAGB) (EDALATI et al., 2022).

Initial studies regarding UFG materials have achieved much higher strengths with these materials in comparison to their Coarse Grained (CG) equivalents. However, since initially UFG materials were synthetized by compacting nano-grained powders, the resulting materials had residual porosity and impurities,

and, therefore, had very low ductility. This paradigm was later changed, with the advance of SPD techniques applied to produce UFG bulk materials. It is now possible to reach these materials, with high strength, wear resistance, high hardness, reasonable ductility, and thermal stability. Also, SPD techniques now allow the production of larger samples, facilitating industrial application and mechanical testing (VALIEV; LANGDON, 2010).

Currently, there is a stablished consensus that materials reach a saturation point after a certain amount of straining, at which, further straining does not result in the decrease of grain size or the alteration of microstructural features. At this stage, an equilibrium is reached, where the formation of defects and their annihilation is equaled. One of the hypotheses for the occurrence of this equilibrium comes from the fact that grain boundaries in UFG materials are sources and sinks of dislocations, which permits the increase in the rate of dislocation annihilation with grain refinement (EDALATI et al., 2022).

There have been different attempts to solve this problem, with the intention of achieving even superior grain refinement. Recent studies observed that less pure metals or composites can achieve smaller grain sizes (and greater thermal stability) due to the occurrence of phase transformations (allotropic and martensitic transitions, formation of grain boundary phases, mass transfer, second phase dissolution or precipitation, and amorphization or crystallization), grain boundary segregation, precipitate formation/dissolution, and texture development (BACHMAIER; PIPPAN, 2019; EDALATI et al., 2022).

Combining SPD techniques, for instance, HPT after ECAP, did not lead to increased grain refinement at the saturation state (LUGO et al., 2008). Cryogenic SPD did achieve smaller grain sizes; however, it led also to inferior microstructural stability at elevated temperatures. Another way to improve properties is to use different materials, high-entropy alloys, for instance, achieved some of the highest recorded hardness in metallic alloys subjected to HPT. Finally, recent studies focused on applying extremely high shear strains through

HPT uncovered new phenomena, which gave rise to the term ultra-SPD (EDALATI et al., 2022).

Among these different approaches, two are of special interest to the present study and will be further discussed. One is the possibility of enhancing mechanical properties through the tailoring of microstructure, using phase transformations and segregation in the grain boundary or dissolving phases and precipitates to achieve supersaturated solid solutions. The occurrence of SPD-induced precipitation or dissolution depends on the initial state of the material, since an equilibrium concentration is found at the steady state of straining, where dissolution and precipitation processes also reach a dynamic equilibrium. This was exemplified by the HPT of Cu-4.9wt%Co alloy samples for the same number of turns, one with previous annealing at 1060°C for 10 hours, leading to almost complete solubilization, and the other, with annealing at 570°C for 840 hours, leading to almost complete Co precipitation. After HPT, an equilibrium concentration of precipitates and solid solution was achieved, as exemplified by the lattice parameter evolution in Figure 4 (MAZILKIN et al., 2019). Higher thermal stability and increased grain refinement have been observed for both precipitation-strengthened alloys and supersaturated solid solutions, which can be explained because grain boundary segregation or precipitates occurring in the grain boundary can act reducing grain boundary mobility, and consequently, grain growth. The same effect occurs for supersaturated solid solutions, but because the decomposition or phase separation is thermodynamically favored over grain growth. The other approach is the application of ultra-SPD (strains above 1000), which have been shown to achieve new levels of steady-state microhardness, ultra-high strength, and high plasticity (EDALATI et al., 2022).

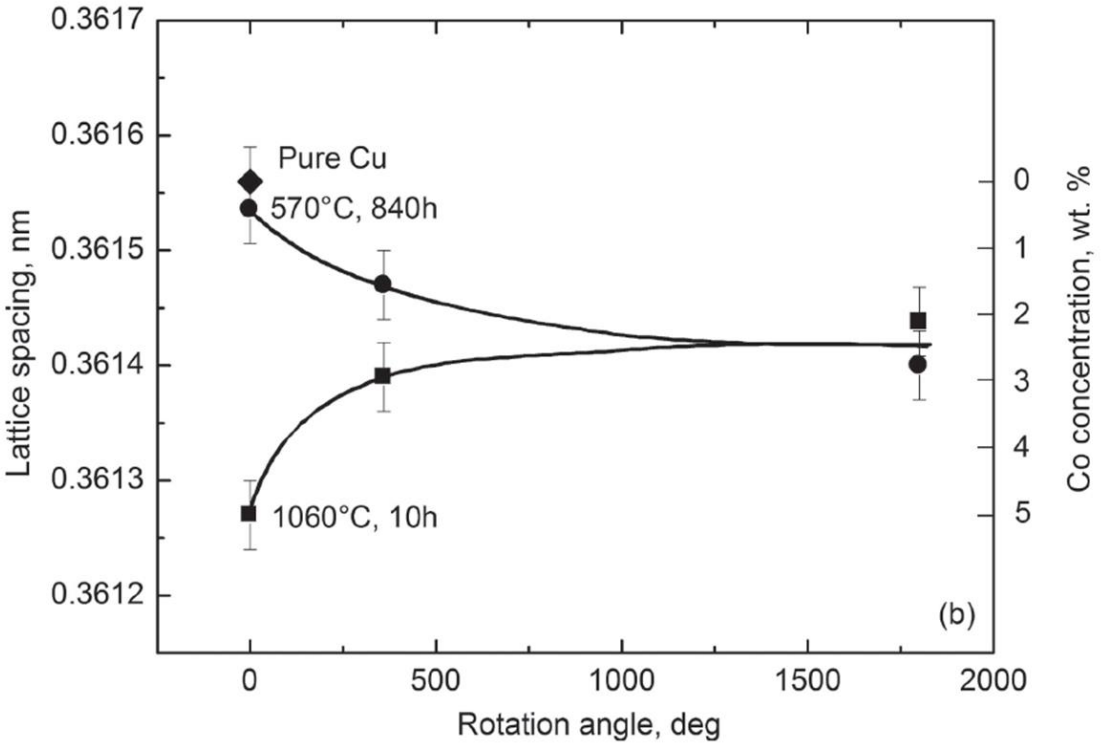

Figure 4: Dependence of lattice spacing on the rotation angle.
Circles mark the lattice spacing in the precipitated sample, annealed at 570°C for 840 h. Squares correspond to the solubilized sample, annealed at 1060°C for 10 h. Diamond shows the lattice spacing for pure copper.
(Adapted from MAZILKIN et al., 2019)

The mechanism of mixing that leads to supersaturation of solid solutions in SPD processed materials has been investigated and the results indicate that it depends on the dissimilarity of strength between the phases. For systems with one much stronger phase, an abrasion-like mechanism is suggested, where the soft phase deforms more and the harder phase fragments. For materials having similar strengths, they can either co-deform, forming lamellar structures or, if shear bands are the main straining route, the structures formed are inhomogeneous (KORMOUT; PIPPAN; BACHMAIER, 2017). When HPT was applied to half-discs of Al and Cu, both supersaturation (of each element in the other's matrix) and the formation of intermetallics (Al_2Cu, AlCu, and Al_4Cu_9), evidenced by X-Ray diffraction (XRD) and energy-dispersive X-ray spectroscopy (EDS) analyses, were observed (OH-ISHI et al., 2013).

Using SPD to produce Metal-Matrix Nanocomposites (MMNC) is a route for achieving enhanced properties and reduced grain sizes that has been receiving some attention lately. For example, consolidation through HPT applied to Al matrix reinforced with Fullerene or carbon nanotube, increased strength and reduced grain size with a reasonable reduction in ductility when compared to the properties achieved in pure aluminum bulk and powder subjected to HPT (ASGHARZADEH; FARAGHI; KIM, 2017; ASGHARZADEH; JOO; KIM, 2014; TOKUNAGA et al., 2008; TOKUNAGA; KANEKO; HORITA, 2008). Similarly, when HPT consolidation was applied to an Al matrix with graphene reinforcement, fragmentation of the graphene nanoplates and refinement of the Al matrix grains occurred, resulting in a nanocomposite with improved hardness, tensile strength, and electrical conductivity (HUANG et al., 2019; ZHAO; LU; GAO, 2015). Reinforcements can act reducing final grain size, e.g., when an Al-Si alloy was subjected to HPT, it presented some regions with disperse fine particles of Si and reduced grains, and other regions without the particles and with larger grains. At the time, this phenomenon was attributed to an increase in temperature due to strain resulting in grain growth. The difference in grain size attained for regions with fine disperse segregations and with coarser precipitates is illustrated in Figure 5 (ZHILYAEV et al., 2007). Another, more recent study, tailored mechanical properties by creating different interface structures resulting in reduced grain size; this was achieved by applying HPT to consolidate Al with reinforcements of Nb_2O_5. Scanning Transmission Electron Microscopy (STEM) investigations using EDS mapping revealed a reduction reaction forming Nb segregations and Al_2O_3 interfacial layers, leading to enhanced properties and reduced grain size compared to pure Al (SILVA et al., 2020).

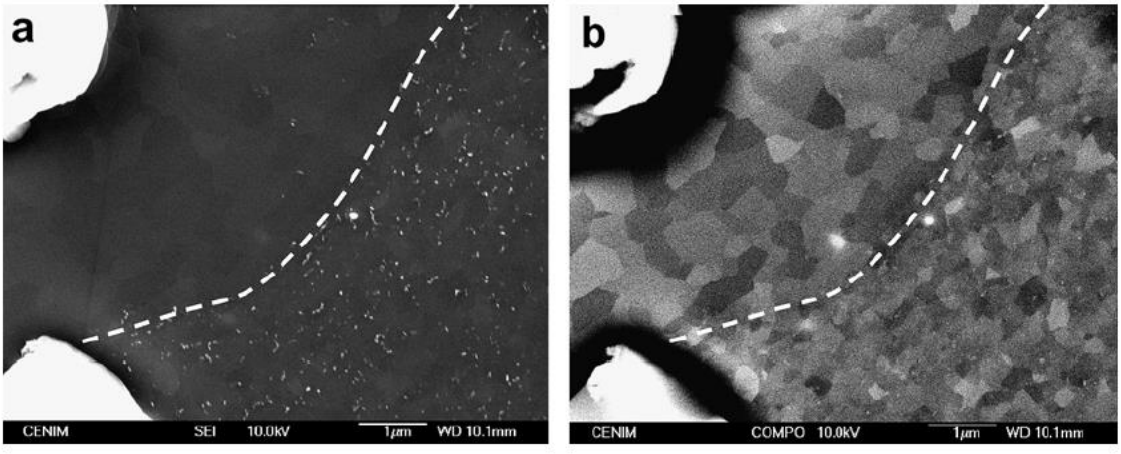

Figure 5: Al-7%Si microstructure after HPT.

SEM image (a) and backscattered image (b) of the same area showing difference in grain size for the particle free zone and the zone with segregations (ZHILYAEV et al., 2007)

The dissolution of a second phase in an alloy during SPD processing, even achieving a supersaturated solid solution and then ageing to achieve fine disperse precipitates, was first attained dissolving cementite in steel (KORZNIKOV et al., 1994). Later, θ’ precipitates were dissolved using ECAP in an Al-1.7at%Cu alloy, and then reprecipitation originated equiaxial θ precipitates on the grain boundaries, where only Guinier-Preston zones were formed prior to SPD (MURAYAMA; HORITA; HONO, 2001).

A different approach than SPD, in the form of mechanical alloying through ball milling, have been deployed on powder materials containing Al and Cu particles, showing that a supersaturated solid solution can be reached. Despite the 0.02at%Cu solubility in Al at room temperature, 2.7at%Cu solubilized in Al has been achieved using mechanical alloying.

X-Ray Diffraction (XRD) is an especially important technique to indicate that Cu has been solubilized, since changes in the reticular constant values and diffraction peaks can indicate the formation of a homogeneous solid solution. However, the use of additional characterization techniques is important to

determine the solid solubility levels and extension with more accuracy (MOLINA-OCAMPO et al., 2016).

Mechanical alloying has also been achieved in the Al-Cu system through SPD itself, using constrained HPT in three stacked discs or quarter-discs, resulting in the formation of multi-layered Al-Cu with vortice-like foldings. The multiphase fine-grained structure led to intensively increased strength, attested by a much higher tensile strength value compared to both Al and Cu after HPT in the same conditions (HAN et al., 2019; KAWASAKI et al., 2018; KORZNIKOVA et al., 2020). The increased hardness achieved by HPT of stacked Al and Cu in comparison to HPT of these pure metals is shown in Figure 6 (KAWASAKI et al., 2018). The formation of vortice-like foldings was observed in HPT of laminate Al and Cu in another study and an explanation to the formation of these structures was provided using finite element modelling (FEM) in the form of plastic instabilities caused by local blocking of shear straining leading to the formation of the vortices. An example of these vortice like foldings observed are shown in Figure 7 (KULAGIN et al., 2018).

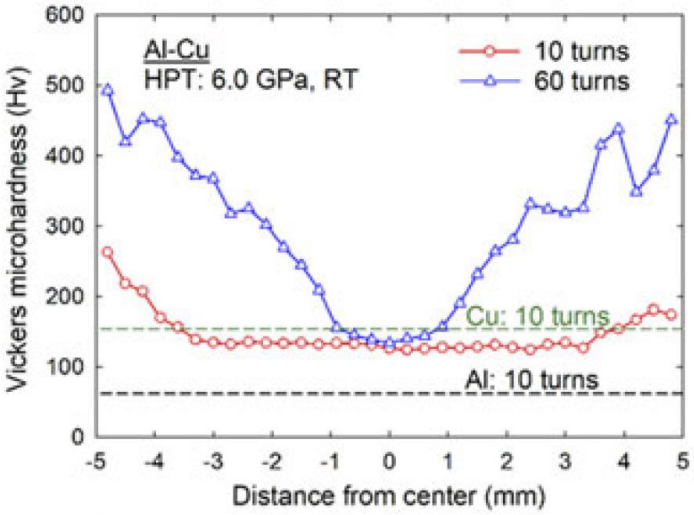

Figure 6: Vickers hardness range for the Al and Cu stacked discs after 10 and 60 turns at 6.0 GPa

(Adapted from KAWASAKI et al., 2018)

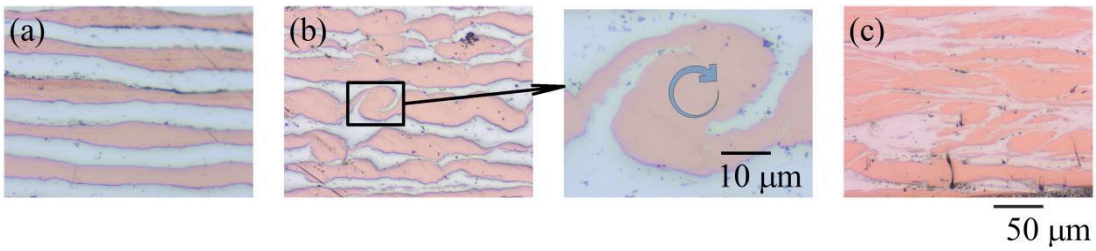

Figure 7: Optical image of the macrostructure of laminate Al-Cu after HPT. In the (a) Centre region, (b) Intermediate and (c) Border region of the sample, with and insert exemplifying a vortice-like folding.
(KULAGIN et al., 2018).

The possibility of achieving excellent superplastic properties is another application of SPD that has been widely investigated since the conditions necessary for these properties to manifest, *i.e*., ultrafine-grained metals with grain size stability at elevated temperatures, can be propitiated by SPD processes (KAWASAKI et al., 2018; KAWASAKI; LANGDON, 2014, 2015; LANGDON, 2009, 2013; VALIEV; ISLAMGALIEV; SEMENOVA, 2007; VALIEV; ISLAMGALIEV; YUNUSOVA, 2001).

Since the discovery of the applicability of SPD to achieve UFG materials with low-temperature superplasticity, in 1988, many interesting material properties obtained by SPD were uncovered, resulting in an increase in researches on the field by the scientific community after the year 2000 (EDALATI et al., 2022). Furthermore, higher strengths than predicted by the Hall-Petch relation were achieved in SPD-processed alloys due to the formation of nanostructures and metastable states. Other important enhancements possible at that time were increased fatigue life and durability, superplasticity, magnetic hysteresis, optical properties for semiconductors, and corrosion resistance (although it was show that corrosion resistance can decrease depending on the nanocrystalline material) (VALIEV; ISLAMGALIEV; ALEXANDROV, 2000). Currently, other interesting functional properties for materials processed with SPD have been achieved, such as shape memory effect, acoustic properties, catalytic activity,

thermal and electrical conductivity, corrosion and radiation resistance, and biocompatibility (EDALATI et al., 2022).

Furthermore, ultrafine-grained (UFG) materials are also potential candidates as raw materials in components fabricated using microforming procedures. Microforming may be defined as the fabrication of parts having at least two dimensions in the submilimetric range. These processes displayed an increasing demand in the last three decades due to their use in the production of sensors, medical equipment, and Microelectromechanical Systems (MEMS) (GEIGER et al., 2001; VOLLERTSEN et al., 2004; VOLLERTSEN; SCHULZE NIEHOFF; HU, 2006). The application of UFG metals in microforming still faces challenges since not much attention has been given yet to the study of formability limitations and failure prediction of severely deformed materials. Nevertheless, it is known that these materials exhibit reduced surface roughness due to grain size related scaling effects. They also help maintain polycrystalline behaviour in micron sized parts and improve material flow in these forming processes, as shown in Figure 8 (BRUDER, 2019).

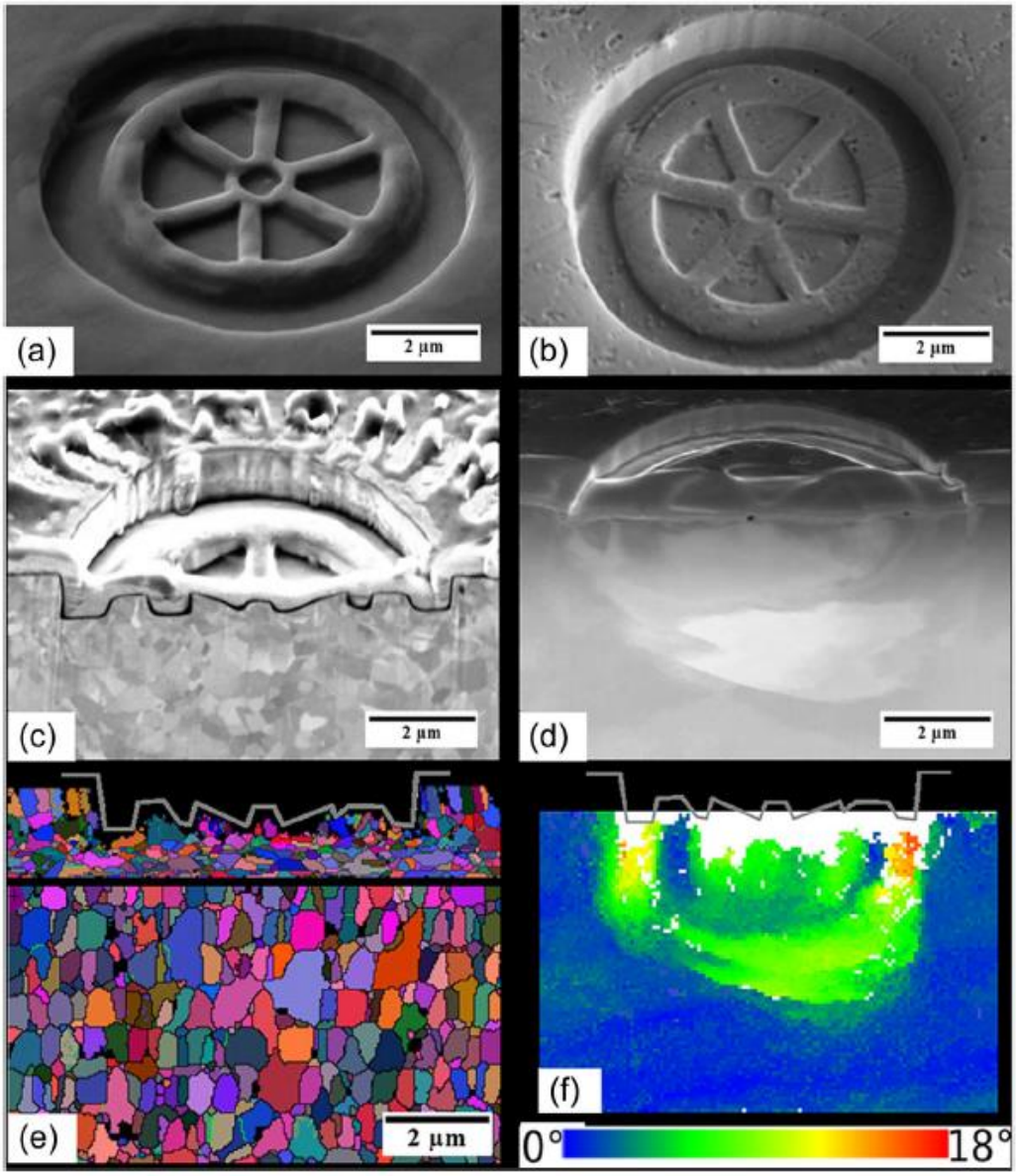

Figure 8: Side-view SEM images of imprints

In (a) UFG-Ni and (b) Single crystalline Ni at depths of about 1 mm, FIB cross sections of imprints in (c) UFG-Ni and (d) Single crystalline Ni, EBSD-scans of the lateral surface of the UFG-Ni cross section (e) directly under the imprint and at a depth of about 10 mm, and (f) EBSD misorientation profile of the SX-Ni cross section. The outer shape of the weel-like indenter is schematically represented by a grey line

(AST; DURST, 2013).

3.2.1 Equal-Channel Angular Pressing - ECAP

Equal Chanel Angular Extrusion (ECAE) or Equal Chanel Angular Pressing (ECAP) is an SPD technique introduced in 1995 (SEGAL, 1995). It can be defined as an extrusion process in which billet is forced through channels of equal transverse section with an angle between them. Throughout the process, the billet is subjected to simple shear uniformly, except for small regions at the ends of the billet. Then, it is possible to repeat the process for more passes, to increase the overall strain. In addition, rotation of the billet between each iteration can be used to enable diverse slip systems and a more homogeneous structure (RADHI; ALJASSANI; MOHAMMED, 2019; SEGAL, 1995). A cross section representation of an ECAP process is shown in Figure 9.

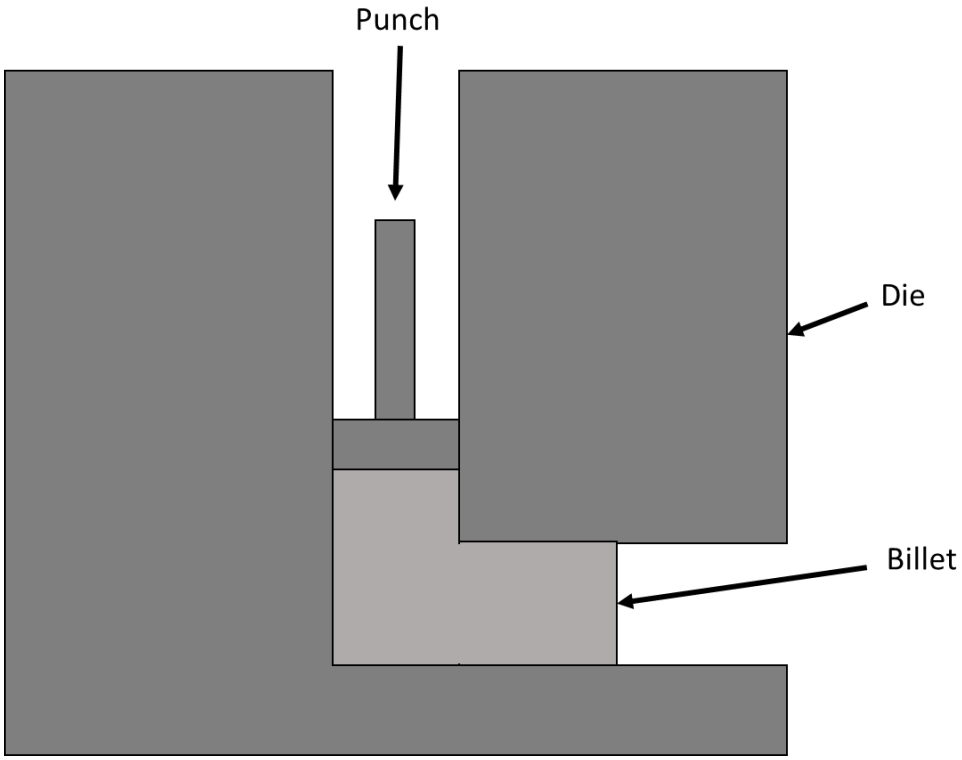

Figure 9: Cross section representation of an ECAP process.

As an SPD technique, ECAP presents advantages, such as the possibility to produce large billets, which permits industrial and structural applications. Also, it is relatively simple, requiring solely a die set, a punch, the billet, and a press, and it is a well stablished method, with many published alternatives for processing routes and procedures, such as rotary dies (VALIEV; LANGDON, 2006). Furthermore, the different processing routes possible with ECAP enables different resulting textures, which affects material properties such as plastic anisotropy, strength, grain refinement, and fracture behaviour (BEYERLEIN; TÓTH, 2009).

3.2.2 Accumulative Roll Bonding - ARB

Accumulative Roll Bonding (ARB) is an adaptation of the rolling process to an SPD technique, to obtain UFG materials. The material is initially rolled and then cut in half; the two resulting sheets are stacked to the height of the initial billet. This process is then repeated successively. After the process, the sheets are bonded, resulting in a bulk material. Furthermore, ARB achieves UFG materials through shear deformation. However, the grains are also elongated similarly to regular rolling (TSUJI et al., 2003).

The bonding that occurs during the process can be explained by the deformation, the increased temperature, and the high pressure on the interface of the sheets. Therefore, it is important to guarantee proper contact between the surfaces, cleaning them thoroughly, removing grease, oxides, and other surface layers. Atomic similarity between the sheets also facilitates the bonding process. However, on the recent years, a significant trend of studying ARB with dissimilar materials or using reinforcement particles has emerged. ARB has the advantages of being the adaptation of a well-known process, requiring only rolling equipment to be performed, and its suitability to manufacture UFG sheets with large dimensions for industrial use (GHALEHBANDI; MALAKI; GUPTA, 2019; TSUJI et al., 2003).

3.2.3 Multi-Directional Forging - MDF

Bridgman proposed a two-directional forging facility with the intention of introducing large strains in metals (BRIDGMAN, 1952; EDALATI et al., 2022); however, Multi-Directional Forging (MDF), as it is currently known, consists of forging a prismatic sample in one direction, and then rotating it and forging it again, successively. Each time the sample is forged and rotated is called a pass, and multiple passes can be performed, maintaining the cross-section geometry, to achieve UFG structures with superior properties (MANJUNATH et al., 2021). A scheme of the evolution of a sample during MDF is shown in Figure 10.

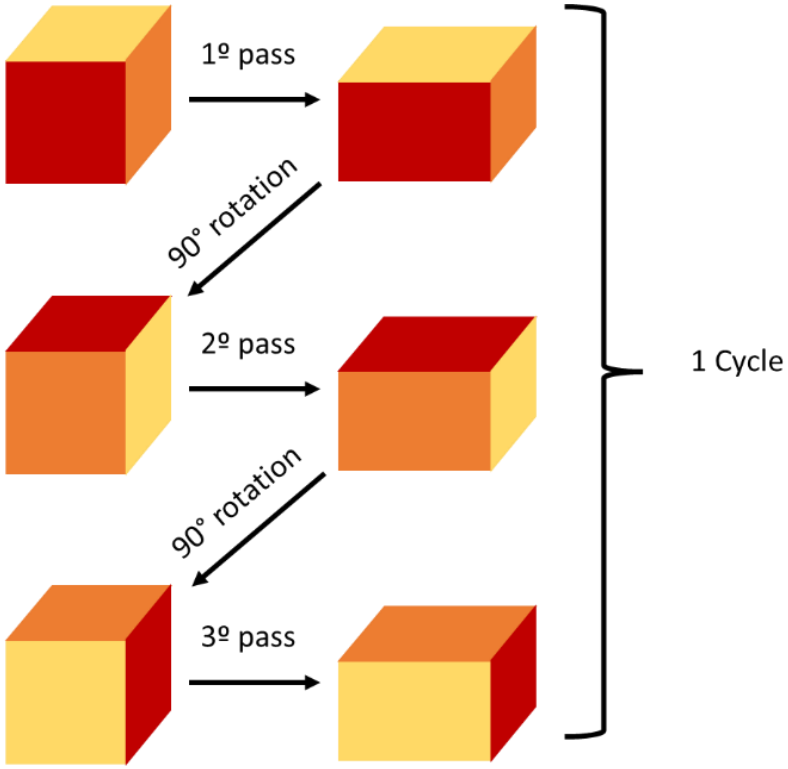

Figure 10: Sample evolution during MDF.

MDF main disadvantages are the occurrence of cracks due to tensile stresses in the free surfaces, which limits the number of passes possible at room temperature, and the heterogeneity of the resulting microstructure, as characteristic of forging processes, mainly because of the friction with the dies (ALTAN; NGAILE; SHEN, 2004; EDALATI et al., 2022). However, MDF is a powerful SPD technique, being the only SPD technique among the most used (ECAP, HPT and MDF) that allows the accurate determination of stress strain curves when re-machining is applied after each compression or when confined plane strain compressions are conducted (Multi-Directional Confined Forging – MDCF) (ALMEIDA et al., 2020; STEMLER et al., 2019). MDF is also capable of achieving impressive properties; when applied to a Cu-Al alloy, MDF resulted in ten times increase of its yield strength because of intense twin formation (DASHARATH; MULA, 2017). Another study with MDF of a Cu-Al alloy resulted in isotropic high strength and high ductility, due to three-dimensional nano-twins (NING; WANG, 2012). However, the Al-Cu alloy usually does not present twins, so the focus is to achieve precipitation hardening. Different studies evaluated the dissolution of second phase (θ') in an Al-Cu alloy and it was shown that MDF achieved the dissolution faster than ECAP due to different stress states (LIU et al., 2010, 2011).

MDF processing was attempted on a two phases Al-Cu alloy (Al-5.5%wtCu), consisting of an α phase, with Cu in solid solution with the Al, and a eutectic phase with composition 67%Al-33%Cu. However, processing was impossible due to fragmentation of the eutectic phase and ultimate failure due to shear band formation (PARIMI; ROBI; DWIVEDY, 2011).

A very interesting perspective is the usage of SPD processing to achieve fine and disperse precipitates in a nano-structured material. A recent study observed that higher temperatures MDF processing followed by ageing treatment resulted in finer, more disperse precipitates and better properties than an aged material without previous deformation by MDF (HE et al., 2018). Other studies used MDF to dissolve θ' or θ'' precipitates in an Al-Cu alloy, then, when an ageing process

was later conducted or nature ageing was allowed to occur, the materials presented an increase in their hardness due to the formation of Guinier-Preston (GP) zones. The much smaller grains after MDF processing provided more sites for heterogeneous nucleation, resulting in finer, disperse precipitates (HUANG et al., 2012a, 2012b). When MDF was compared to HPT on an Al-4%Cu binary alloy, HPT resulted in a more homogeneous microstructure, with a smaller in-equilibrium grain size and higher Vickers microhardness (XU et al., 2013).

3.2.4 High-Pressure Torsion - HPT

HPT was the first SPD technique ever introduced (BRIDGMAN, 1935). It consists of subjecting a disc to high hydrostatic pressure in between two anvils, allied with shear straining generated by torsion created by the rotation of one of the anvils. Three main categories of HPT can be defined regarding constraining configurations. In the constrained configuration, the disc is completely constrained inside the HPT facilities, completely restraining material flow in the radial direction. In the quasi-constrained configuration, the anvils have grooves similar to those used in the closed die forging process, however, material flow to the flash is restricted but not prevented. Finally, in the unconstrained configuration, the anvils contact surfaces are plane, with no restriction to radial material flow, except for friction forces (PEREIRA; FIGUEIREDO, 2019). A scheme of the transverse view of HPT comparing the three possible constraining configurations is presented in Figure 11.

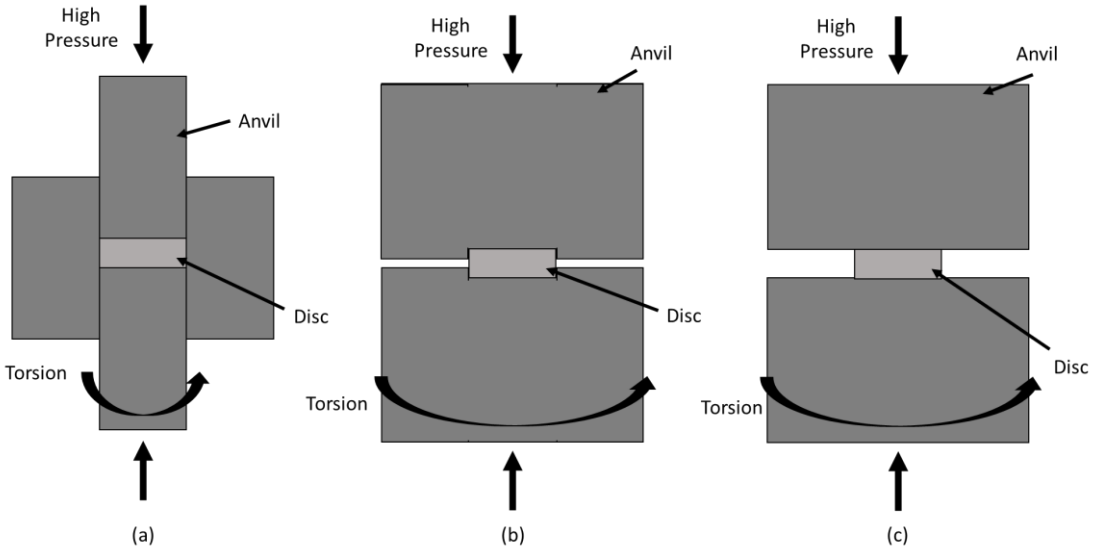

Figure 11: Scheme of HPT processes.
(a) constrained; (b) quasi-constrained; and, (c) unconstrained configurations.

It has been shown that the Finite Elements Method (FEM) is a viable tool to represent the plastic flow, microstructural evolution, pressure distribution, and temperature variations in HPT processes. FEM is also a valuable tool to understand the effects of the variation of geometrical factors and friction conditions. Evaluation of the three constraint configurations using FEM indicated that the quasi-constrained configuration has the best compromise between dimensional control and torque requirements (PEREIRA; FIGUEIREDO, 2019).

Initial studies applying HPT were mainly focused on polymorphic phase transformations under high pressure; however, many different classes of materials, such as oxides, glasses, ceramics, pure elements, alloys, and minerals, were subjected to experiments with HPT, and the finding of the possibility to consolidate occurred very early on, after the proposal of HPT, with an article from 1936 by Bridgman himself, proposing that coherent discs would result from HPT applied to fine powder materials (BRIDGMAN, 1936; EDALATI; HORITA, 2016). Another very important finding by Bridgman was that the strain hardening effect was not indefinite, achieving saturation for very high shear strains (BRIDGMAN, 1935). This proved a disagreement to the power-law proposed by Zener-Hollomon, for very high strains (ZENER; HOLLOMON, 1944).

Other phenomena uncovered by Bridgman's studies were the possibility of strain softening, indications of dynamic recrystallization at large strains because of the rarity of amorphization, material dependency (melting point and crystallization capacity for minerals) on the refinement under severe strain, occurrence of new phases, and the acceleration of phase transformations (EDALATI et al., 2022).

The principle used in HPT that permits SPD and the achievement of UFG materials is that, due to the small geometrical changes that occur during torsion, the torsion fracture strain is higher than those of other loads, for instance, tensile loading. Furthermore, the high hydrostatic pressures that are also used can raise the fracture strain to infinity (PIPPAN et al., 2008). This combination of intense hydrostatic pressures and high shear strains is beneficial for grain refinement, powder consolidation, and the occurrence of solid-state reactions (EDALATI et al., 2022). Recent studies applied ring constraints of harder materials than the powders to be consolidated by HPT, and identified, through experimental results and FEM simulation, that a back pressure is generated, increasing hydrostatic pressure and contributing to the consolidation of the powders (JOO; KIM, 2016; KHAJOUEI-NEZHAD et al., 2017).

HPT is a very popular SPD technique because of its inherent advantages, such as the possibility of continuous variation of strain, instead of stepwise; its suitability for easily achieving very high strains; the possibility of controlling strain rate and temperature of the process; and, applicability for brittle materials (PIPPAN et al., 2008). Other main advantages of HPT are that high hydrostatic pressure can prevent the formation of cracks during straining, enhance the kinetics of phase transformations, and lead to mechanical alloying not achievable by classical metallurgy through cold consolidation and diffusion bonding. Additionally, HPT processing leads to the highest defect concentration among all SPD techniques, since the pressure hinders defect annihilation (EDALATI et al., 2022).

These advantages make HPT a great process for studying the effects of high strains in materials, however, disadvantages such as size limitation (due to the maximum applicable pressure determined by the hardness of the tools) and heterogeneous material properties (because of strain dependency on the distance from the centre) hamper industrial application. The equivalent strain in an HPT process relative to the distance from the centre can be calculated by the following relation (VALIEV et al., 1996):

$$\varepsilon = \frac{2\pi n r}{\sqrt{3}t} \quad (2)$$

where ε is the equivalent strain, n is the number of turns, r is the distance to the centre, and t is the thickness of the sample.

The size limitation regarding the samples produced by HPT makes it so that tests have to be adapted to smaller sizes in comparison to those suggested by norms. The Plane Strain Compression (PSC) Test has been subjected to such miniaturization and experiments coupled with FEM simulations demonstrated it to an effective tool to obtain stress strain curves of samples subjected to HPT. Furthermore, the PSC would be specially suited for initially particulate samples, since the compression would hinder crack formation, as opposed to the tensile test (CARVALHO et al., 2022; FORD, 1948).

An example of metallic alloying through HPT was achieved for a Cu-53at%Fe powder mixture. Despite the immiscibility of the system, the resulting alloy presented two phases, a Cu FCC phase with approximately 20%at Fe dissolved in it, and a Fe Body-Centred Cubic (BCC) phase with approximately 25%at Cu dissolved in it (BACHMAIER et al., 2012; EDALATI et al., 2022).

Strain-induced precipitation has been observed for a low Cu Al-Cu alloy, in which particles precipitated, segregated to the grain boundaries, and later were fragmented with increasing strains (NASEDKINA et al., 2017). A recent study employed up to 200 turns HPT in tri-layered Al-Cu-Al and found that the strain led to the formation of a lamellar structure, and later fragmentation and dissolution of both Al and Cu in the other matrix occurred. This study also reported the

formation of Al_2Cu and Al_4Cu_9 phases (BAZARNIK et al., 2020). Other studies using layered, half or quarter discs Al-Cu also reported the occurrence of lamellar structures, fragmentation, and formation of intermetallics such as Al_2Cu, Al_4Cu_9, and AlCu (BOUAZIZ; KIM; ESTRIN, 2013; DANILENKO et al., 2018, 2019, 2021; HAN et al., 2018; KHISAMOV et al., 2022; OH-ISHI et al., 2013). The solid-solubilization process has been shown for a powder mixture of Cu-Cr to result mainly of mechanical mixing and fragmentation, which increases with strain (BACHMAIER et al., 2014). It has been shown that ageing can be employed after SPD procedures in low Cu Al-Cu alloys and result in better strength properties than merely employing SPD or ageing (GOODARZY et al., 2014).

Figure 12 shows SEM images of the phase distribution of an Al-Cu-Al stack subjected to 10 revolutions of HPT, and it is possible to observe the stretching of the Cu phase, followed by fragmentation and further stretching. Similarly, Figure 13 shows a TEM image, associated with SAED results and a SEM image with EDS analysis of an Al-Cu-Al stack subjected to 20 revolutions. From those images it is possible to observe that the SAED analysis associated with the TEM image revealed the precipitation of Cu in the Al, in the form of Al_2Cu, furthermore, the SEM image shows a clear flow instability in the form of a vortice-like structure.

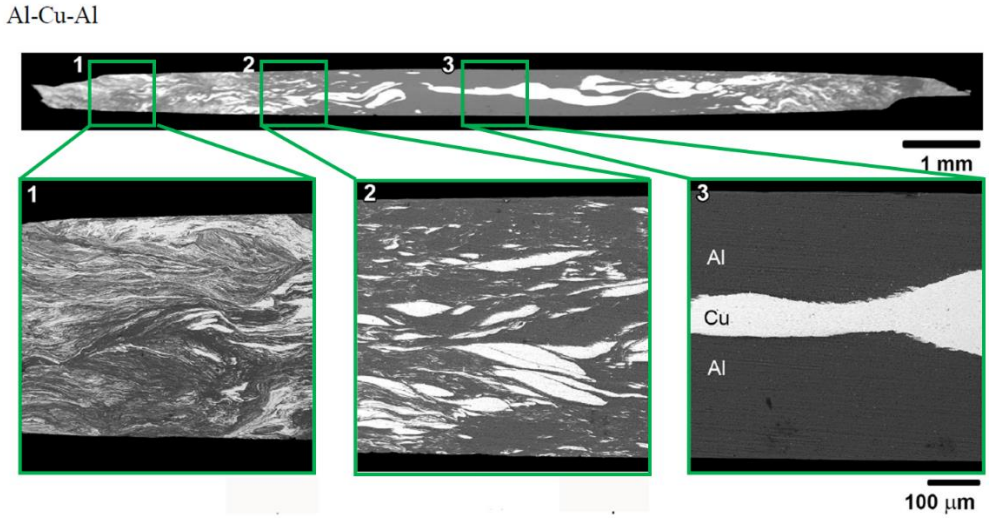

Figure 12: SEM images of the transverse section of an Al-Cu-Al stack sample subjected to 10 HPT revolutions (adapted from DANILENKO et al., 2018).

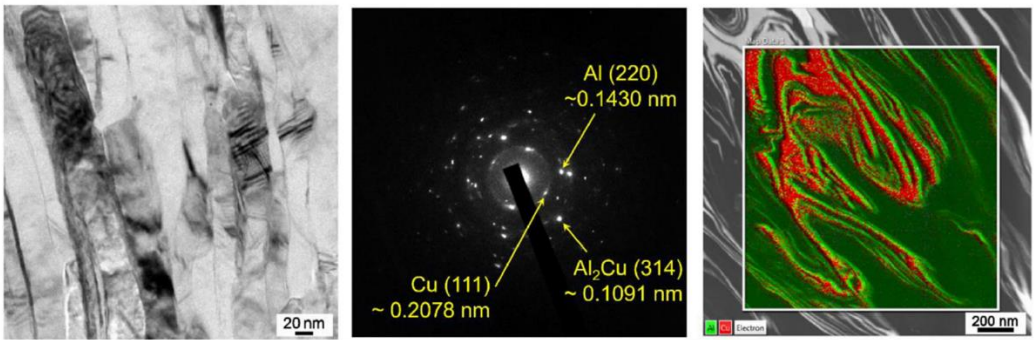

(a) (b) (c)

Figure 13: *Analyses conducted on the border region of an Al-Cu-Al stack sample subjected to 20 revolutions of HPT (a) TEM, (b) SAED and (c) SEM.*

4 Experimental Materials and Procedures

4.1 Materials

The materials used were 98.6% purity aluminium powder, with 350 mesh granulometry (particle diameter < 45 μm), and 99.5% purity copper, with 150 mesh granulometry (particle diameter < 100 μm).

4.2 Processing

The Al and Cu powders were hand mixed with ~4% weight composition. This composition was chosen because of its possibility of solubilization under conventional solubilization treatment and the availability of other studies with similar compositions. The necessary mass of each element was calculated using their density and the final volume of the desired 10 mm diameter by 1 mm height discs. The mixed powders were cold pressed using a plunger through a round channel of a massive die using a compressive load of ~30 kN (axial pressure ≈ 400 MPa). The discs were then subjected to quasi-constrained HPT processing (FIGUEIREDO; CETLIN; LANGDON, 2011; PEREIRA et al., 2014; PEREIRA; FIGUEIREDO, 2019) at room temperature (RT ≈ 300 K) using anvils displaying shallow depressions of ~8 mm in diameter. First, the workpieces were compressed within the anvils using a nominal pressure of ~6 GPa. Afterwards, the lower anvil was rotated at a constant rate of ~1 rpm for numbers of turns (N) of 1, 3, 10, 30, 60 or 100.

4.3 Microstructural Characterization and Mechanical Testing

After the HPT processing, samples were grounded, polished with 1 μm diamond paste, and then the Vickers microhardness distributions were measured along

one diametral line for each sample. The value in each position was calculated as the mean of the measurements of 4 indentations, each 0.15 mm away from the calculated position. The indentations were conducted using a FM-700 tester equipped with a Vickers indenter, using 100 gf for the 1 and 3 turns samples and 300 gf for the rest. The dwelling time was 10 seconds. A scheme of the method used is presented in Figure 14 (DOS SANTOS et al., 2023; KAWASAKI; LANGDON, 2008; MACHADO et al., 2023)

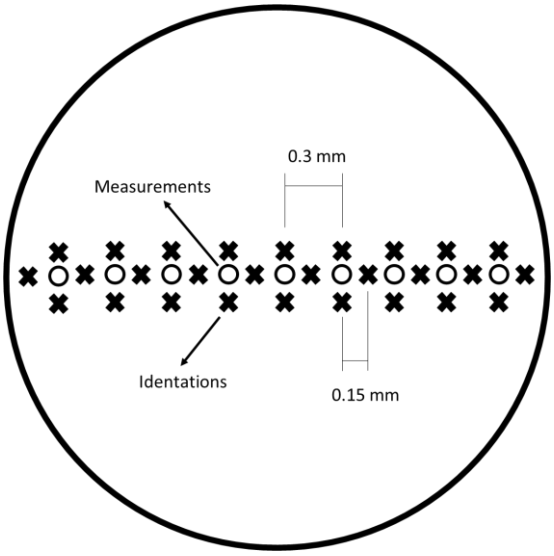

Figure 14: Scheme of the method used to obtain the Vickers Microhardness measures.

Samples processed for 1, 30 and 100 turns were grounded with abrasive paper #240 on the circular faces and on two sides, until the distance between the sides was 7 mm, in order to obtain a rectangular contact area for the PSC test. A Shimadzu Autograph AGS-X universal tester was used to conduct two PSC tests on each sample with a tool that had a breadth of 1.4 mm. After the tests, post-mortem images of the samples were taken using an Esferium X4 USB digital microscope. Figure 15 shows a schematic representation of the tool and samples used in the PSC tests (CARVALHO et al., 2022).

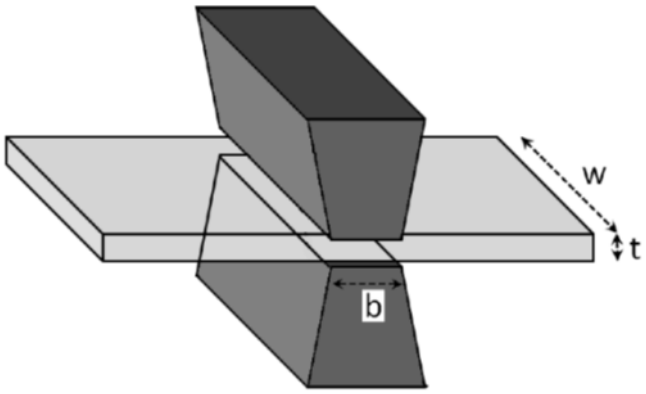

Figure 15: Schematic representation of the PSC test, where “b” is the tool breadth, “w” the sample width and “t” the sample thickness (adapted from CARVALHO et al., 2022)

After the same preparation used for the microhardness test, SEM was conducted on samples processed for 1, 30 and 100 turns using a FEI Quanta 200 FEG microscope. The presence of pores, phase distribution and indentation size correlation with the phase distribution were assessed generally and, on the center, and border regions. EDS analyses were also conducted following one radial for each sample, to estimate the Cu distribution on the aluminum matrix.

XRD analyses were conducted on samples processed for 0.1, 1, 3, 10, 30, 60 and 100 turns, after the samples were prepared by grounding one surface of the discs with abrasive paper #1200. The analyses were performed with a Phillips PANalythical C’Pert Pro diffractometer with Co Kα1 (λ = 1.5406 Å) radiation. The XRD patterns were recorded on the prepared surfaces of the discs through θ-2θ scans undertaken from 2θ = 10–90° using a time step of 3 s and an angular increment of 0.02°/step. The resulting diffractograms were used to calculate the lattice parameter, crystallite size and microstrain using “Material Analyses Using Diffraction” (MAUD) software (LUTTEROTTI; SCARDI, 1990; RIETVELD, 1969).

Lastly, TEM lamellae were extracted from discs processed for 1, 30 and 100 turns using Focused Ion Beam (FIB) milling on a FEI Quanta 3D FEG microscope. The milling of the lamellae was conducted on the discs surfaces, with the lamellae

length following a radial direction, at the border-most regions of the samples. For the 1 turn sample, the lamella was milled in such a way to include the interface between a Cu phase and the Al matrix and EDS mapping was conducted. The extracted lamellae were subjected to TEM analyses on a FEI Tecnai F20 microscope operating at 200 kV to examine grain size and particle size and distribution. Particles compositions were examined using SAED. A scheme of the processing and characterization techniques used on the samples is presented in Figure 16.

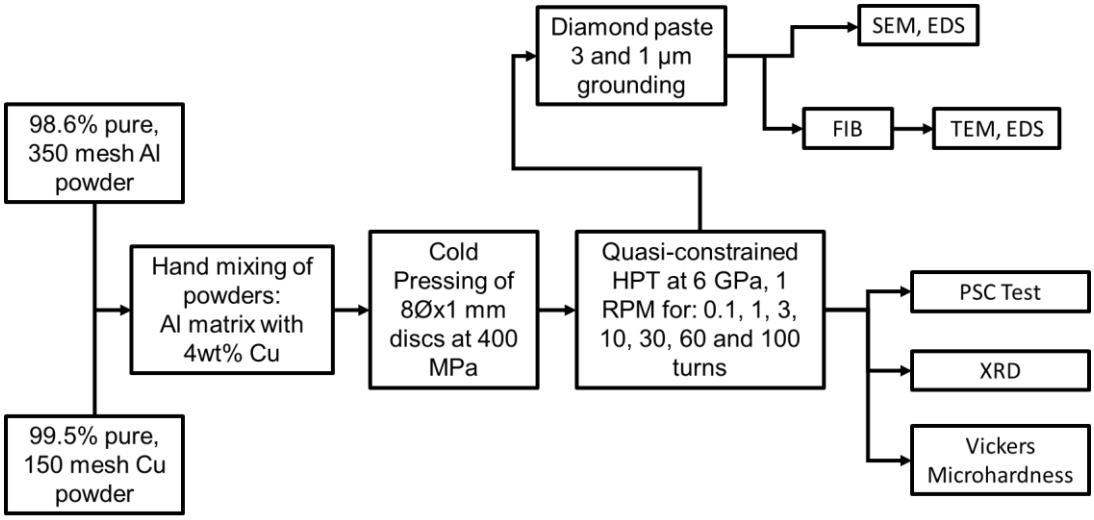

Figure 16: Flowchart of the processes, analyses and tests used on the studied samples.

5 Results and Discussion

Results for the Vickers Microhardness distribution and SEM analysis are presented in this section. Comparisons of the Vickers Microhardness as a function of the distance from the centre are shown in Figure 17.

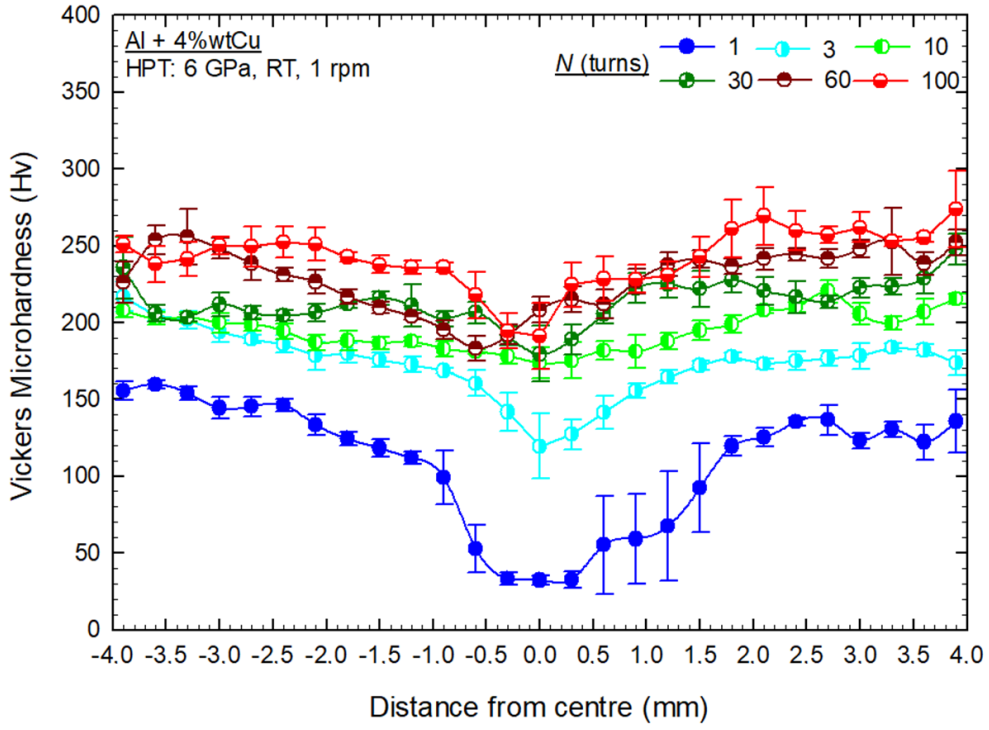

Figure 17: Vickers Microhardness as a function of the distance from the centre for the Al-Cu mixture after different numbers of HPT turns.

Observing these results, it is possible to assert the occurrence of some trends. Firstly, the increase in the number of turns resulted in an increase in the hardness values and a more homogenous distribution of hardness. Secondly, the material processed by one turn exhibits low hardness values (< 50 Hv) at the disc centre which suggests an insufficient consolidation of the metal powders. There is a sudden increase in the hardness at radial positions (r) close to 1.0-1.5 mm and the hardness continues to increase with increasing radii and reaches ~150 Hv at r > 3 mm. Lastly, it is apparent that the material does not reach a saturation

condition as the Vickers microhardness continues to increase with increasing numbers of turns and achieves an upper bound of ~270 Hv at the disc edge after processing through 100 turns.

Figure 18 shows plots of σ vs ε for Al+4wt%Cu discs processed by 1, 30 and 100 turns of HPT and further subjected to PSC testing at RT. Images of the post-mortem workpieces are also shown for comparison purposes. It follows from these plots that the material processed by 1 HPT turn displays a yield strength of ~200 MPa and this increases to ~300 MPa after HPT processing by up to 30 and 100 revolutions. For all conditions, the Al+4wt%Cu alloy exhibits significant strain hardening and achieves maximum flow stresses of ~500, ~750 and 850 MPa for N = 1, 30 and 100 turns, respectively.

After reaching these stresses, there is a rapid drop in the loads during testing and the material fails by the onset and propagation of cracks. These cracks are visible in all deformed specimens and the ultimate failure occurs at lower strains for the discs subjected to higher numbers of turns. It should be noted, however, that the Al+4wt%Cu alloy processed by one HPT turns exhibits several small cracks within the deformed surfaces. These cracks are associated with the local drops in the flow stress in the curve shown in Fig. 18 which are likely triggered by the presence of a higher number of cavities in the processed metal but which was not sufficient to cause catastrophic metal failure during PSC testing.

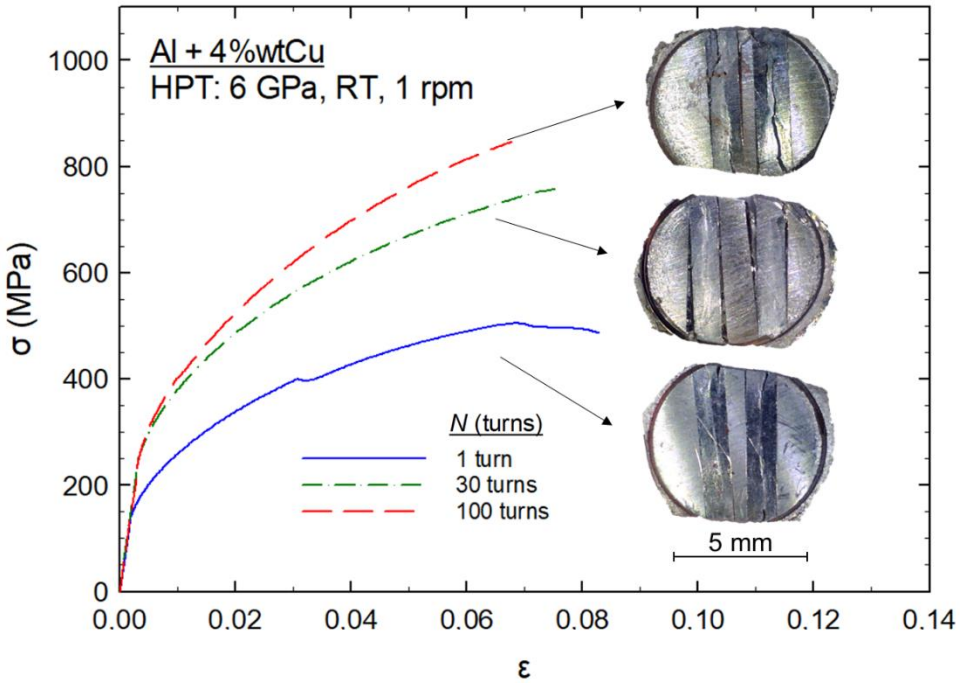

Figure 18: Equivalent stress (σ) vs equivalent strain (ε) curves of the Al+4wt%Cu alloy processed through 1, 30 or 100 HPT turns and further tested under plane strain compression. The images of the deformed discs are also portraited as inserts.

Backscattered electrons (BSE) SEM images were extracted for each sample, first, with a small magnification, showing larger regions of the samples, and then, with increased magnifications at the centre region and at the border region. An example of the images taken for the 1 turn sample is shown in Figure 19. For the other samples, relevant images were selected to demonstrate phenomena that occurred.

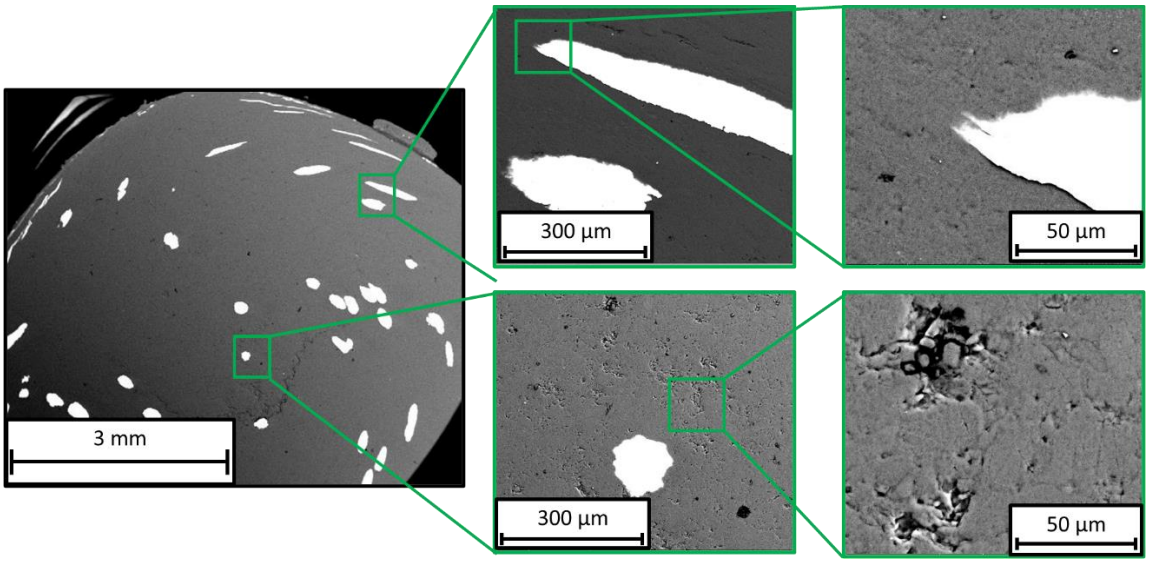

Figure 19: BSE SEM images for the 1 turn sample with different magnifications.

It is possible to observe that the copper is distributed as a second phase in the Al matrix, in the form of globular particles closer to the centre and more elongated particles closer to the border. Also, there are pores in the sample, indicating that complete consolidation was not achieved. These pores are more prevalent closer to the centre, which is a result of the lower strains in the center of the sample. A comparison of a broad region for all the samples that were subjected to SEM analysis is shown in Figure 20.

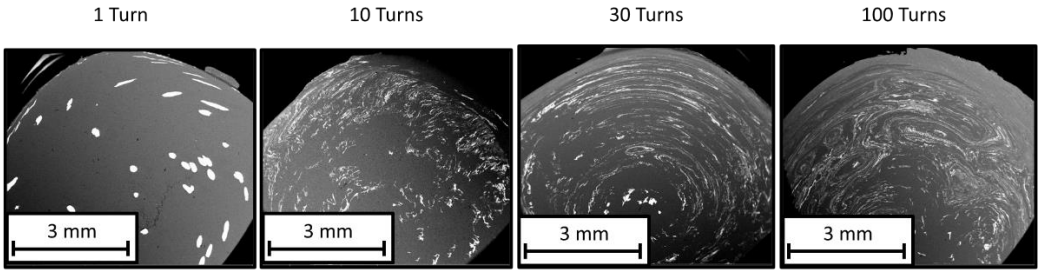

Figure 20: SEM analysis of all samples, BSE SEM images.

Analysing the results in Figure 19, it is possible to affirm that mixing of the Cu phase occurred as the number of turns increased, forming lamellar structures, indicating that co-deformation occurred, which is reasonable, since Al and Cu have similar strengths. These lamellar structures were mostly aligned with the circumferential direction, however some regions experienced vortice-like foldings, evidencing flow instabilities. A comparison of the centre regions of the 1 and 10 turns samples is shown in Figure 21, with measurements of the reinforcement phases and pores.

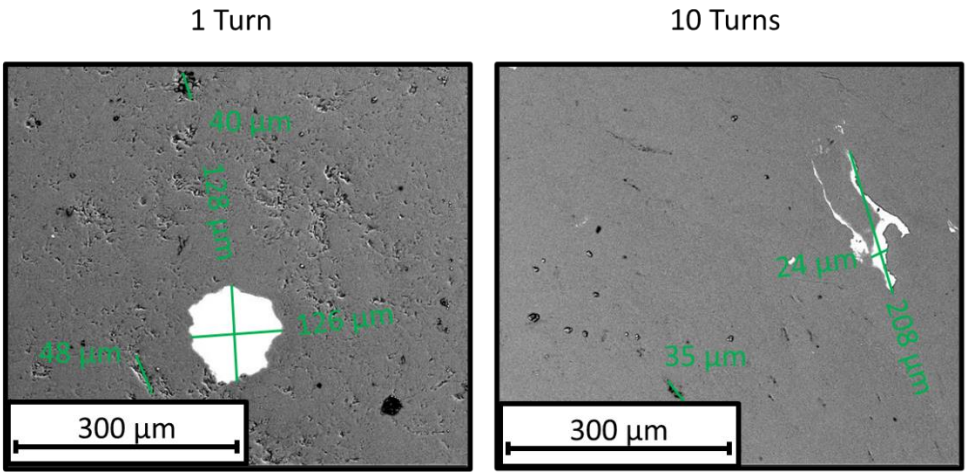

Figure 21: Centre region comparison for 1 and 10 turns samples, BSE SEM images.

The 10 turns sample had less and smaller pores; beyond that, for samples with more turns, the amount and size of the pores became similar and negligible, indicating that complete consolidation has been achieved. The 10 turns sample showed smaller, more elongated second phase particles in the centre region in comparison to the 1 turn sample.

Secondary Electrons (SE) SEM images and EDS analyses for the 1, 30 and 100 turns samples are presented in Figure 22. From these analyses the lighter

structures observed on the matrix were confirmed to be Cu particles and it was determined that they are heterogeneously distributed along the surface of the disc for the 1 turn sample.

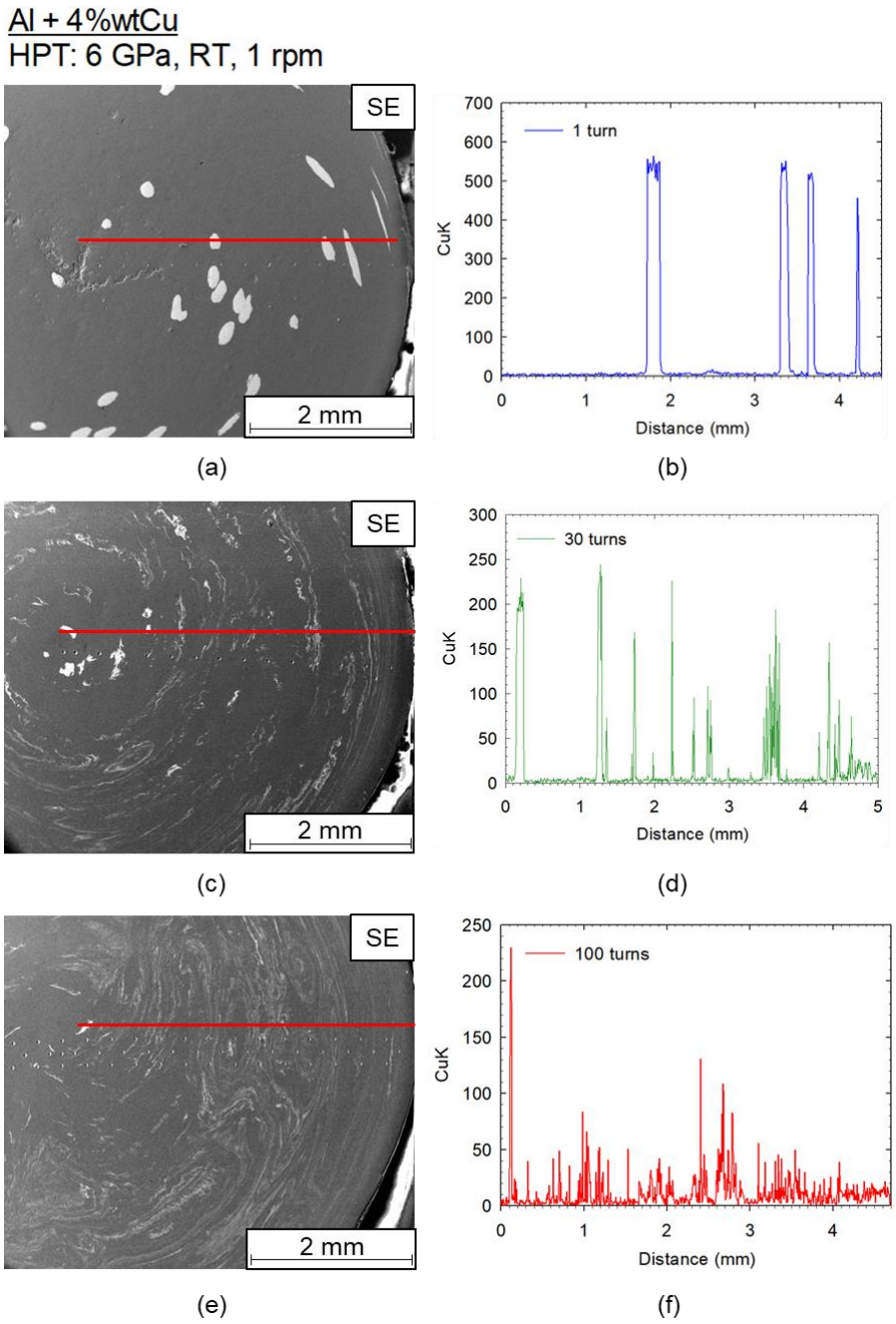

Figure 22: SE micrographs and corresponding EDS line scans

revealing the overall distributions of Cu-rich particles throughout the surfaces of the Al+4wt%Cu discs after processing by (a,b) 1, (c,d) 30 and (e,f) 100 HPT revolutions.

It is evident that the Cu particles are severely stretched with increasing strain, and therefore, numbers of turns. Thus, they cover the whole mid-sectional surfaces of the discs and they are sometimes arranged in the form of vortex-like structures (JIANG et al., 2020; KULAGIN et al., 2017). This follows from the SE images and the EDS line scans of the material deformed up to 100 revolutions in which there are Cu peaks along the entire scanned line, although they became less intense by comparison with the other HPT conditions. The overall shape and size of the Cu domains at different radial positions is depicted in detail in the SEM images in Figure 23.

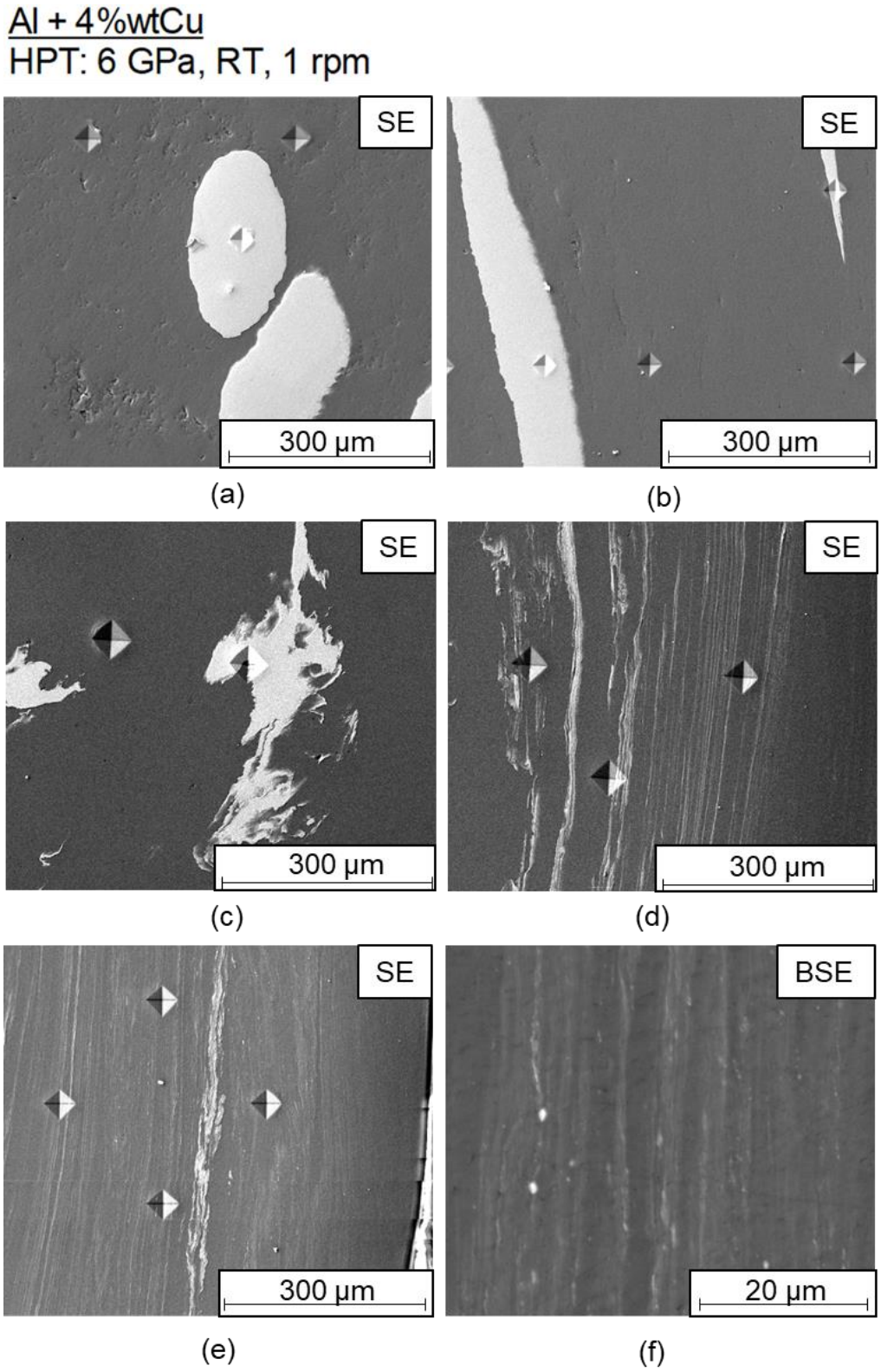

Figure 23: SEM micrographs showing the shapes and sizes of Cu-rich particles at the centres (a,c) and at the outer radial positions (b,d,e,f) of the Al+4wt%Cu discs after processing by (a,b) 1, (c,d) 30 and (e,f) 100 HPT revolutions.

It is readily seen in Figures 23 (a and b) that there are several microcavities throughout the Al matrix after 1 HPT turn. These cavities are associated with lower hardness values that correspond with the larger indentation sizes encountered in these areas. The microvoids become elongated and scarcer at the outer regions of the disc and are virtually absent in the material processed by 30 and 100 revolutions. A thorough examination of the indentation sizes in Figures 23 (a,b) also shows that the Cu particles are harder than the Al matrix at positions located close to the disc centre after processing by 1 turn. Conversely, for similar radial positions, the differences among the indentation sizes become less distinguishable with increasing numbers of HPT revolutions.

The results displayed in Figure 23 demonstrate that the Cu powders are gradually deformed and fragmented with increasing HPT straining. After the achievement of a critical level of consolidation of the Al powders, the round Cu particles which are initially hundreds of micrometres in size are stretched out in the shearing direction. This is followed by a severe reduction in thickness for the Cu domains which display dimensions in the range of ~10-100 μm and ~1-10 μm after 1 and 30 revolutions, respectively, at the outer regions of the discs.

It follows from the BSE image in Figure 23 (f) that the long Cu bands are eventually fragmented into several particles with sizes in the submicrometre range. Also, their surroundings exhibit brighter colour hues than the grey matrix which may indicate the dissolution of Cu into aluminium as already reported for other Al systems after HPT processing (DOS SANTOS et al., 2023; ZHANG et al., 2019a, 2019b). It is important to highlight that this phenomenon may contribute to the achievement of further hardening in the Al+4wt%Cu alloy because the indentations imprinted in these areas display smaller sizes.

Figures 24 - 26 shows a distribution of indentations along the radial direction for the 1, 30 and 100 turns samples respectively, presenting the hardness values measured for each of those indentations. From these images it is possible to observe that the hardness values are significantly higher on the Cu particles while

those are still large enough to accommodate an indentation, however, the difference in the hardness of the particles compared to the hardness of the surrounding matrix reduces with increasing strain. Furthermore, it is possible to observe that the hardness increase significantly and reach their maximum once the disperse distribution is achieved.

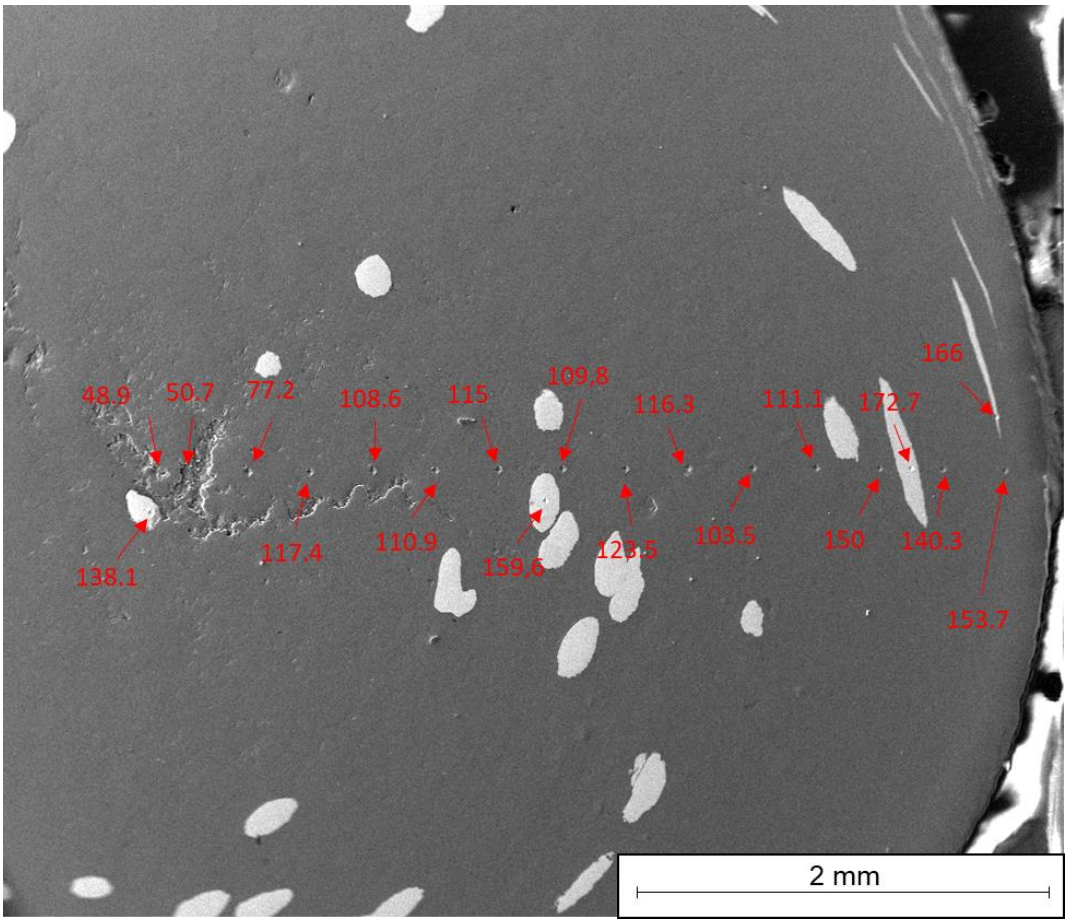

Figure 24: Hardness distribution for the 1 turn sample.

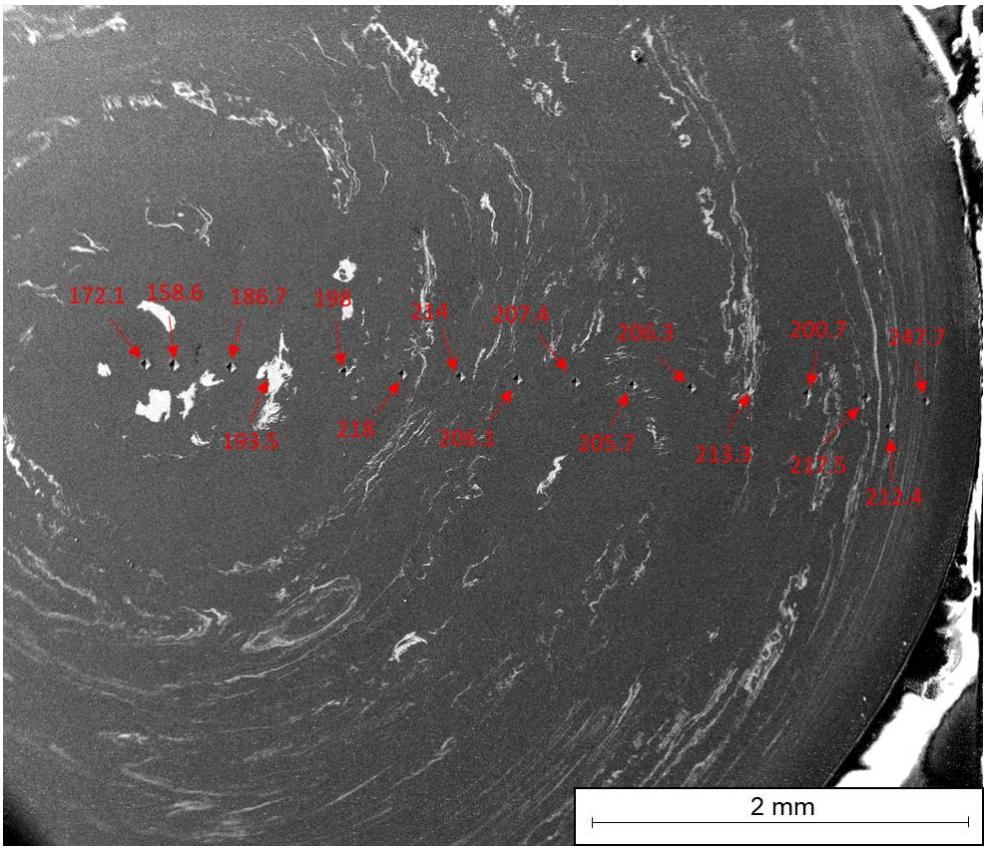

Figure 25: Hardness distribution for the 30 turns sample.

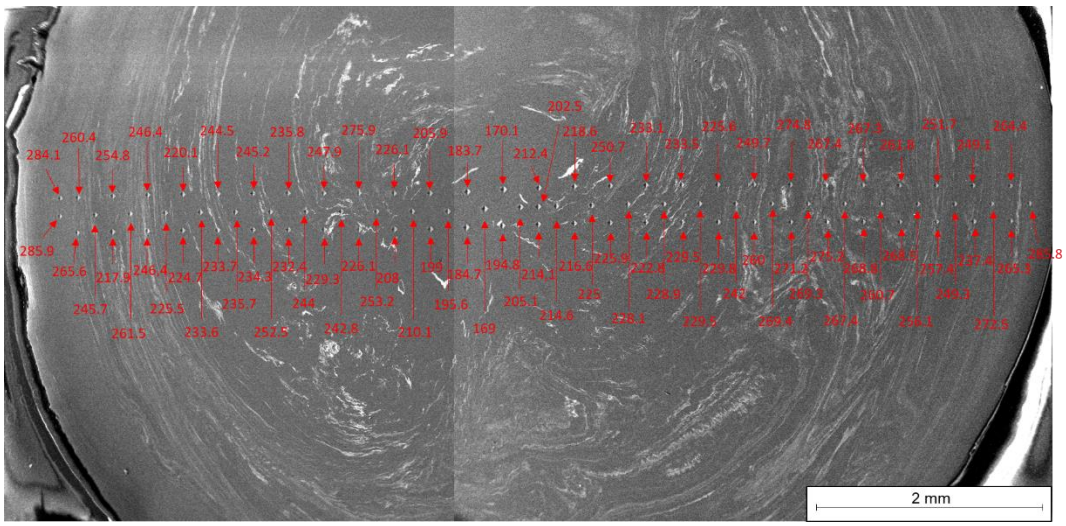

Figure 26: Hardness distribution for the 100 turns sample.

Figure 27 shows the X-ray diffraction patterns obtained for the samples. From these results, it is possible to observe that the initially identifiable Cu phase for 1-10 turns is not identifiable after 30 turns, which is probably a result of the intense stretching and fragmentation of the Cu particles with increasing strains. Also, from these diffraction patters the lattice parameter, crystallite size and microstrain were estimated.

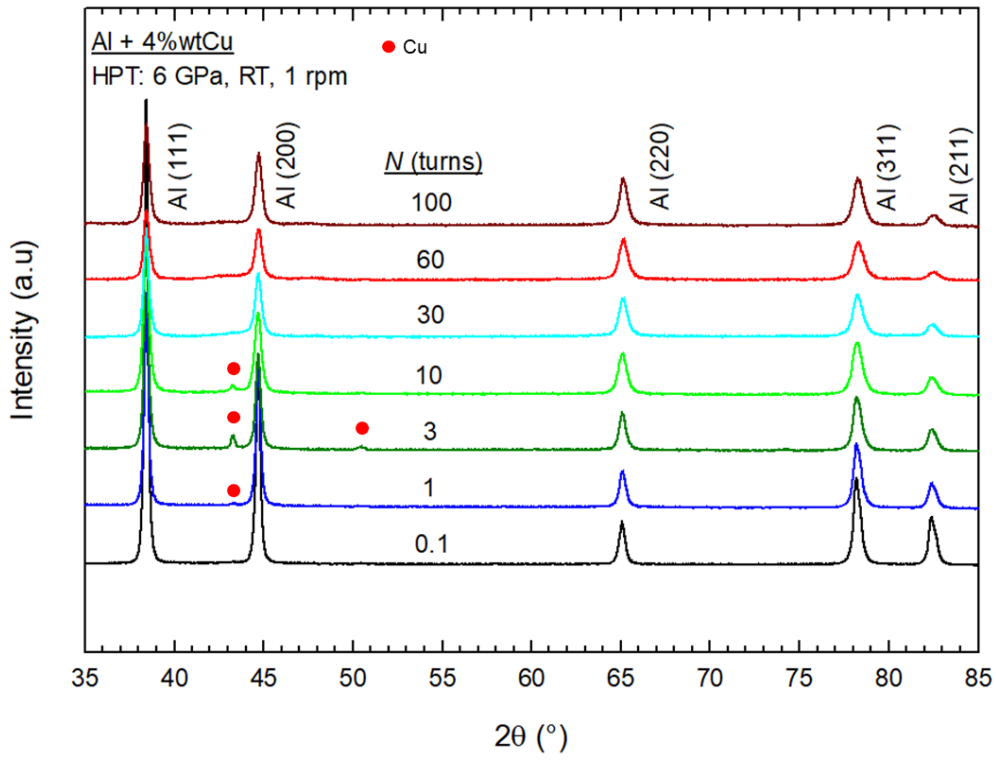

Figure 27: X-ray diffraction patterns.

Figure 28 shows the variation of the lattice parameter, the average crystallite size and the microstrain with the numbers of turns for the Al+4wt%Cu discs processed by up to 100 HPT revolutions. It is readily noted that the lattice parameter estimated using the XRD measurements shows a decreasing trend with additional plastic straining up to the attainment of 60 HPT turns. This may indicate the partial solubilisation of Cu in the Al matrix as reported elsewhere (BAZARNIK et al., 2020; BOUAZIZ; KIM; ESTRIN, 2013; LIU et al., 2010;

LUBARDA, 2003; MURAYAMA; HORITA; HONO, 2001; OH-ISHI et al., 2013). From this processing stage onwards, the lattice parameter calculated for the Al+4wt%Cu mixture stabilises at ~4.047 Å. The microstrain increases and the crystallite size steadily decreases with increasing HPT straining up to *N* = 10 turns. Further deformation does not significantly affect the values estimated for these parameters such that the Al+4wt%Cu compound achieves a crystallite size of ~50 nm and a microstrain of ~2 × 10^{-3} after 100 revolutions.

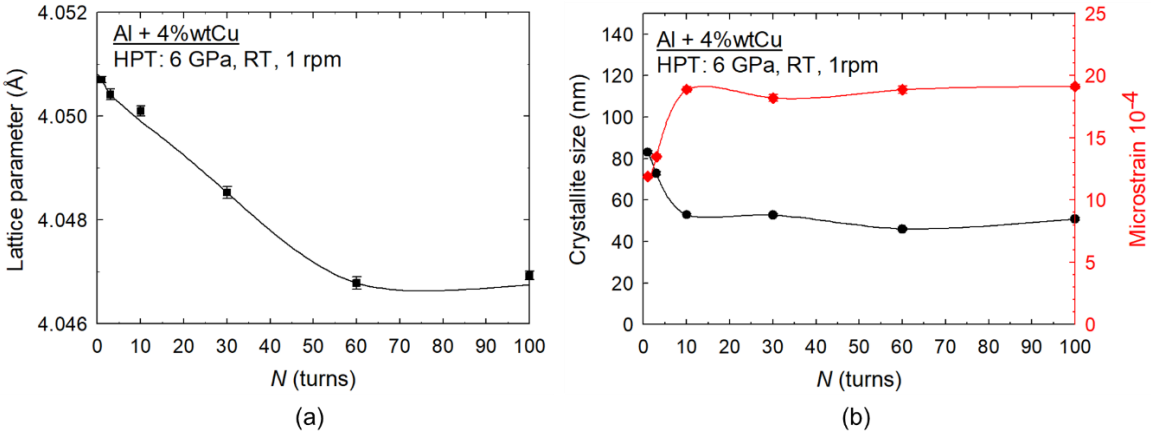

Figure 28: (a) Lattice parameter, (b) crystallite size and microstrain as a function of number of turns for Al+4wt%Cu discs processed by up to 100 HPT turns.

Figure 29 shows representative bright field (BF) TEM images and corresponding SAED patterns taken at selected positions for the microstructures of the Al+4wt%Cu alloy processed by one HPT revolution. The structures in Figure 29 (a) correspond to an area located within the Al matrix, separated by a large distance from any Cu particle, whilst the regions with bright contrast in Figures 29 (b, c) are also composed by Al but are much closer to a relatively large Cu particle. All SAED patterns display a ring-like shape which suggests that the crystallites within these areas are separated mostly by boundaries having high misorientation angles.

It is readily apparent that the grains of Al near the Al-Cu interface have high aspect ratios and are stretched out along a direction parallel to their nearest Al-

Cu contour. On the other hand, the grain structures far from the Cu particles are less elongated and exhibit larger sizes but within the submicrometre range. For both regions a few of the Al grains contain internal dislocation structures and they appear to be in an earlier stage of dynamic recovery in areas far from the Cu domain.

The region with a dark contrast in Figure 29 (c) belongs to an elongated Cu particle located at the outer radial position of the disc subjected to 1 HPT turn, as follows from the EDS map in Figure 29 (e). It is evident that the grains within these regions have ill-defined boundaries and display larger sizes than the Al grains. Also, the Cu domain shows a much higher density of tangled dislocations than the Al matrix. After 1 HPT turn, the mean sizes of the Al and Cu grains are ~110 and ~220 nm, respectively, as determined using the linear intercept method. The EDS maps in Fig. 29 reveal the presence of an O-rich layer at the Al-Cu interface on the Al side. This was probably present in the original surfaces of the Al powders and was identified as Al2O3 through indexation of the SAED pattern.

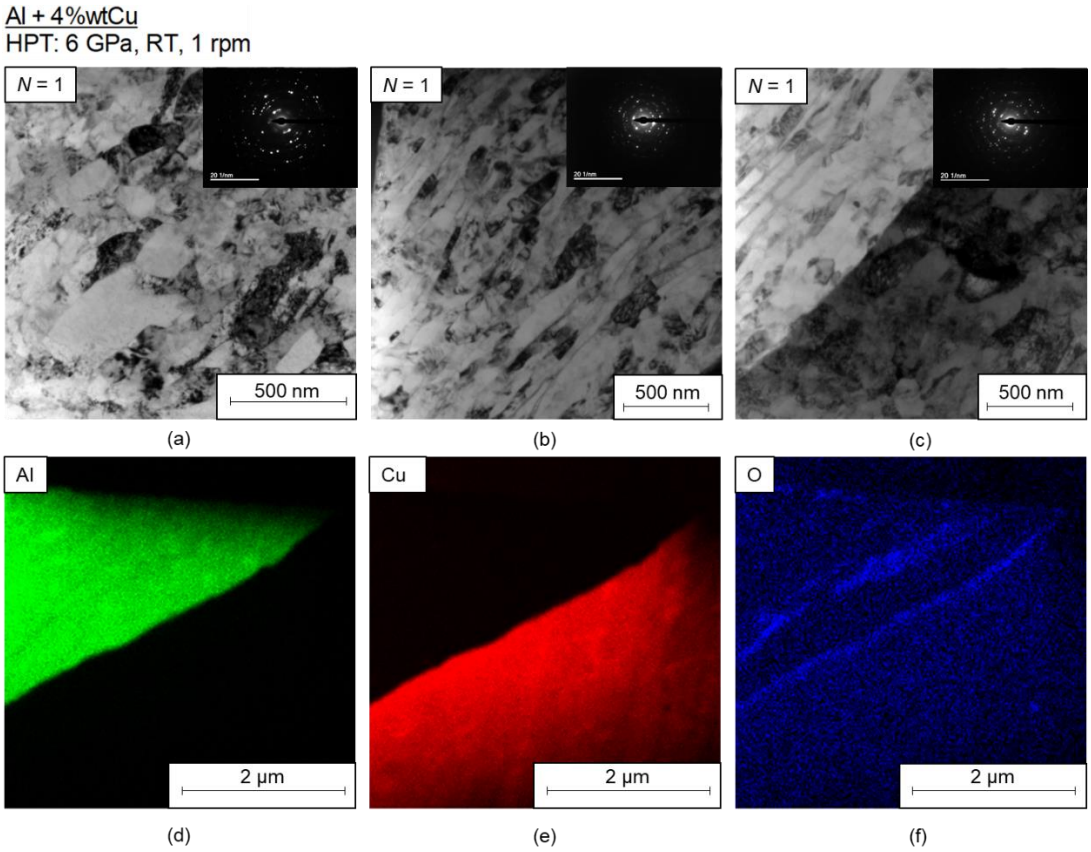

Figure 29: TEM images and SAED patterns for 1 turn sample. At positions (a) distant or (b,c) in the vicinity of an Al-Cu interface for the Al+4wt%Cu alloy processed by 1 HPT turn. The EDS maps for (d) Al, (e) Cu and (f) O are included for the same area analysed in (c).

The Al grain structures of the Al+4wt%Cu alloy synthesised through processing by up to 30 and 100 HPT turns are depicted in the bright (BF) and dark field (DF) TEM images in Figure 30. After 30 and 100 turns, the HPT-processed discs exhibit uniform arrays of grains with average sizes of ~55 and ~48 nm, respectively. The grains of Al in the material subjected to 30 turns display a lower amount of dislocations than after 1 revolution and they are slightly elongated towards the shear direction. By contrast, after 100 HPT turns the Al grains are not aligned with any specific direction but instead they are apparently distributed in a whirlpool-like pattern, as follows from Figure 30 (d).

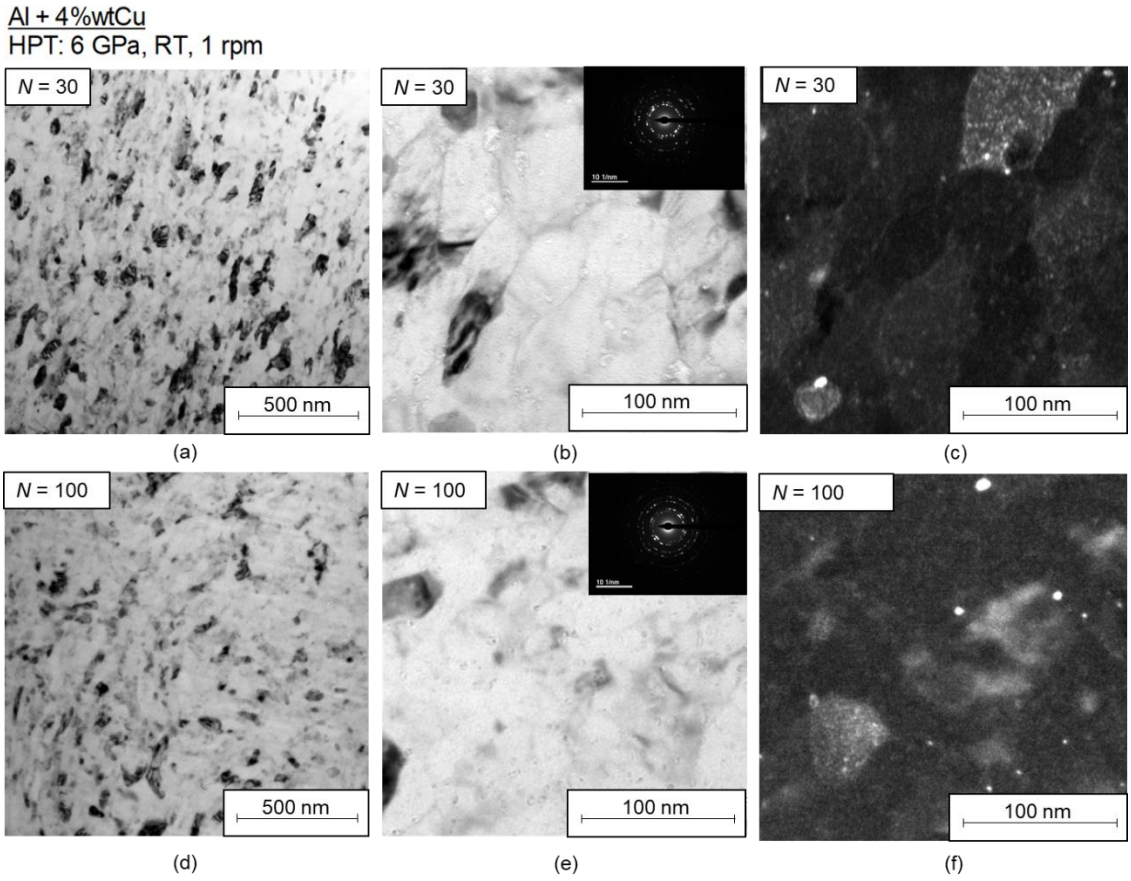

Figure 30: TEM images and SAED patterns for 30 and 100 turns samples. At different magnifications showing the grain structures of the Al+4wt%Cu alloy processed through either (a,b,c) 30 or (d,e,f) 100 turns of HPT.

Inspection of both the BF and the DF TEM images reveals the presence of a homogenous distribution of nanosized second phases in the microstructures of the alloy processed by 30 and 100 turns. These particles are more easily visualised in the DF images in which they present a bright contrast. To better visualise the size, shape and distribution of these nanoprecipitates, Figure 31 displays TEM images with higher magnifications for the Al+4wt%Cu alloy processed by up to 1, 30 and 100 HPT revolutions.

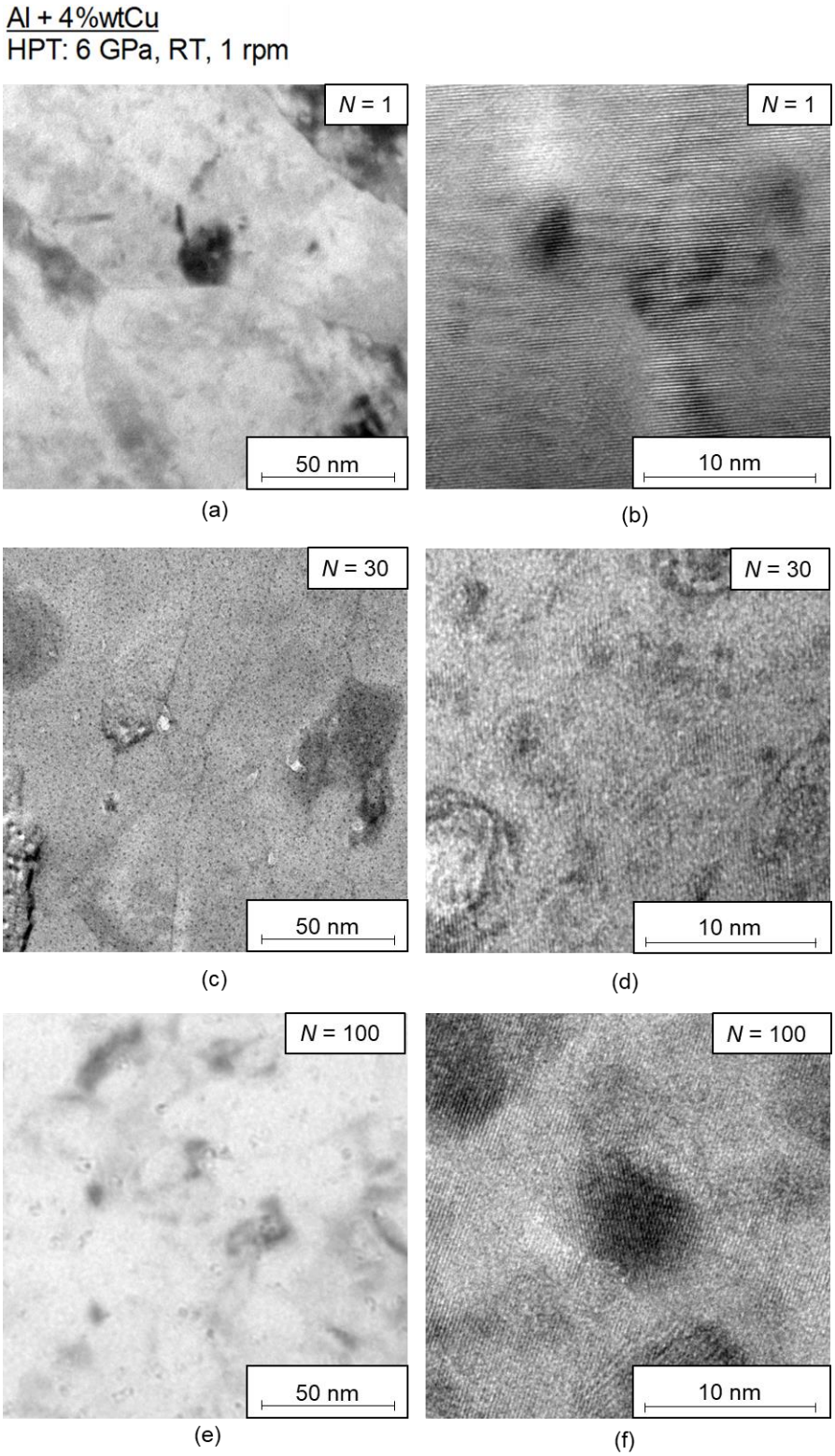

Figure 31: TEM and HRTEM images showing details of the precipitates of the Al+4wt%Cu alloy processed by (a,b) 1, (c,d) 30 and (f,g) 100 HPT revolutions.

It should be first noted that the material deformed up to one HPT turn already displays a few round particles close to the interface with the large Cu domain as shown in Figure 29 (c). It follows from the HRTEM results in Figure 31 (b) that the precipitate boundaries are coherent with the Al matrix and have diameters of less than 10 nm. An examination of various SAED patterns at these areas indicated that the nanosized particles correspond to Al_2Cu precipitates representing GP zones or θ'' precipitates (HAN et al., 2018; NASEDKINA et al., 2017).

The TEM images in Figures 31 (c,d) clearly demonstrate that the nanoparticles display much smaller sizes and are more abundant in the alloy subjected to 30 revolutions. After 100 turns, the number fraction of precipitates diminishes by comparison with the material processed by 30 HPT turns. Furthermore, the second phases display larger sizes and this leads to a loss of coherency with the Al matrix as is evident in Figure 31 (f).

The size of the nanoparticles depicted in several TEM images were measured through the equivalent circle diameter method in Image J software by counting more than 200 individual precipitates in each HPT condition and the datum points were used to construct the histograms depicted in Figure 32. It is important to note that, after one HPT turn, the particles in the Al matrix are mostly encountered near the Al-Cu interface and exhibit an average size of ~5.4 nm. The number of particles per area (n_p/A) increases by one order of magnitude and reaches ~0.03 nm^{-2} in the Al+4wt%Cu alloy processed by 30 revolutions. They also become notably smaller and exhibit a mean diameter of ~2.0 nm. On the other hand, further straining up to N = 100 leads to a significant increase in the size and a decrease in the number fraction of nanoprecipitates.

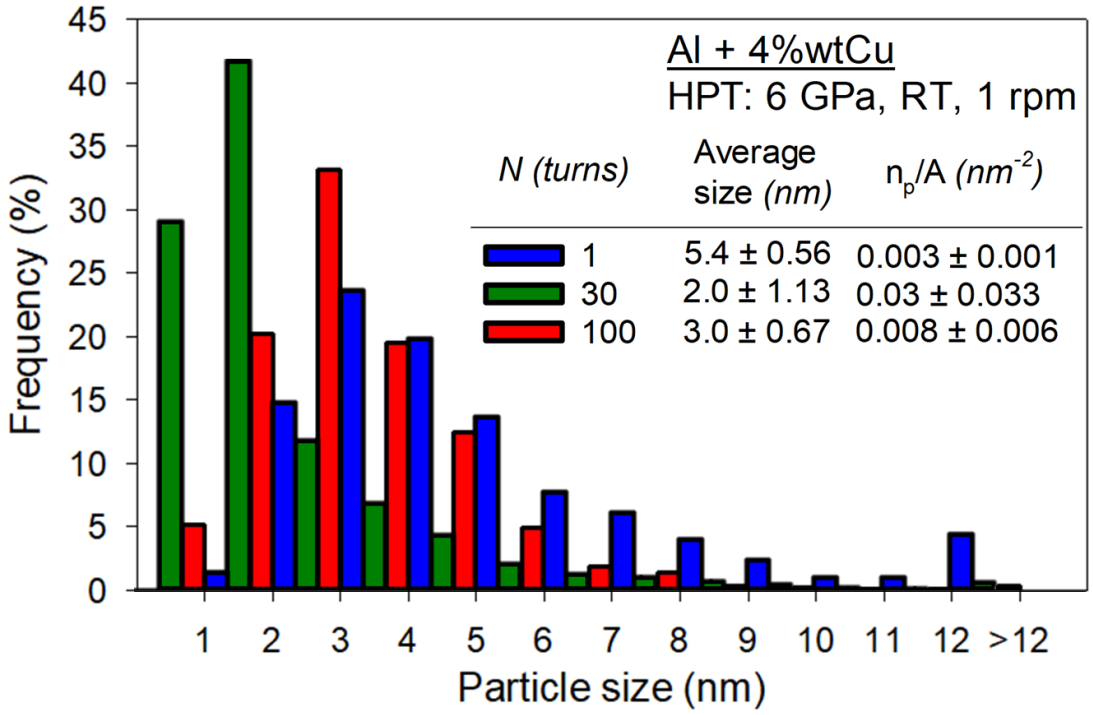

Figure 32: Histograms revealing the size distributions for the Cu-rich particles encountered in the Al+4wt%Cu alloy processed by up to 100 HPT revolutions.

The results presented until now demonstrate that HPT processing successfully promotes the consolidation of dissimilar metal powders constituted by Al and Cu through a complex series of events at the micro and nanoscale involving the stretching and fragmentation of Cu particles up to a point in which the Cu is partially solubilised and eventually precipitates within the Al-matrix. To summarise the current findings and permit a comprehensive discussion concerning the various solid-state reactions observed in the Al-Cu nanocomposite synthesised through HPT, Figure 33 shows a pictorial representation of the redistribution of the mixing phases and the nanostructures developed in the edge of the discs processed by up to 100 revolutions.

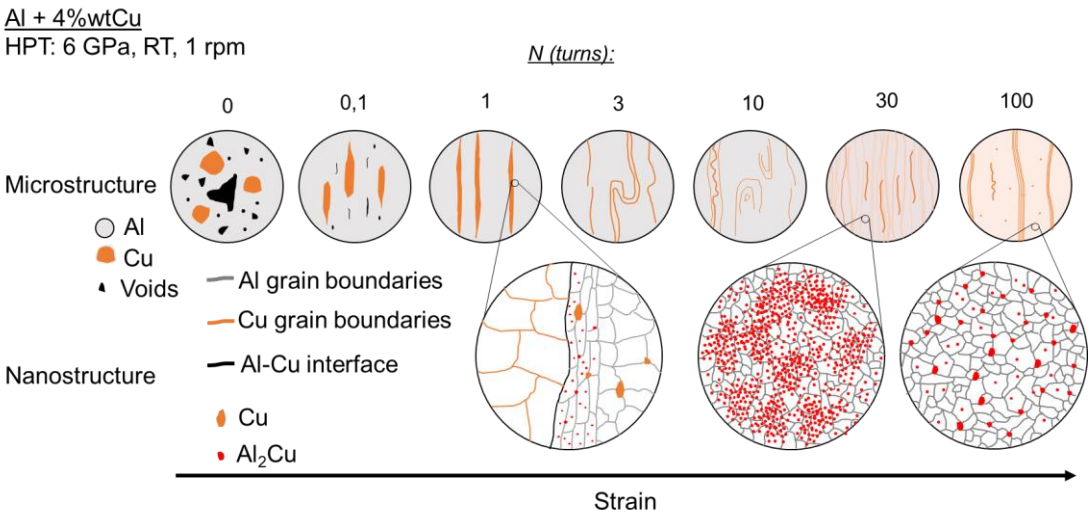

Figure 33 Schematic representation of the mixing and fragmentation of metallic powders and the tailored microstructures for the Al+4%wtCu alloy synthesized through HPT processing by up to 100 revolutions.

Prior to HPT processing, the cold-pressed powders displayed many voids. The combination of elevated hydrostatic pressure and torsional straining led to the closure of the microcavities which are no longer detected at the borders of the disc after 1 turn but remain present at the centre (Figure 23). For this reason, the material subjected to one revolution is not fully consolidated and exhibits lower hardness values at its central area. In addition, the presence of microvoids triggers local cracking in the early stages of PSC testing as follows from the stress drops and cracks in Figure 18. Therefore, after 1 HPT turn the Al-Cu composite is not yet suitable for any practical applications which require an improved load-bearing capacity.

Furthermore, there is evidence of plastic deformation in the Cu domains that are slightly stretched along the circumferential direction of the disc processed by one HPT turn. Nevertheless, if strain partitioning had occurred equally in both phases, the Cu particles at any given position would cover nearly the entire circumference of the sample, which is hardly the case for this composite. It is evident in Figure 22 (a) that the Cu particles at inner radial positions continue portraying a round

shape and, even though they are clearly stretched at the disc edges, each individual domain has a length of <2 mm.

It is thus consistently shown that plastic straining may concentrate in local areas of the Al matrix and this may even accelerate the process of grain refinement in aluminium, as supported by the finer grain structures encountered in the vicinity of the Cu particles for the material processed by 1 turn of HPT (Figure 29). This phenomenon is also reported for other multiphasic alloys such as dual phase steels and its origin is associated with the development of micro shear bands within the softer phase (SILVA et al., 2023; TASAN et al., 2014).

Additional deformation promotes the hardening of the Al matrix surrounding de Cu particles and both phases eventually reach similar flow stresses. This favours a new balance on strain partitioning towards a more substantial deformation in copper which shows good agreement with the long strips found in the microstructure after 30 turns. After sufficient straining, the Cu strips are fragmented into short bands or even round particles with sizes of < 1 μm as demonstrated in Figure 23. There is also evidence for the formation of Cu whirlpools due to the onset of flow instabilities similarly to the flow patterns encountered in recent studies (HUANG; KAWASAKI; LANGDON, 2013; JIANG et al., 2020; KULAGIN et al., 2017). Finally, it is revealed that the areas near the fragmented particles have a brighter contrast than at earlier processing stages.

These observations suggest that, although a few Cu fragments continue mono-constituted, straining generally promotes the partial dissolution of Cu into the Al matrix. This is supported by the decrease in the lattice parameter with increasing numbers of turns as shown in Figure 28 (a) for data refined from the XRD spectra. It should be noted that the spectra were acquired along the entire mid-sectional surfaces of the discs in which they underwent different levels of strain depending on their radial positions (VALIEV et al., 1996). Nonetheless, the lattice parameter was also calculated through measurement of the radii of the Al rings of several SAED patterns for the Al-Cu alloy processed by 1, 30 and 100 turns. These

results correspond to radial positions next to the disc edges and they reliably confirm the reduction of the lattice parameter in the Al-Cu solid solution with increasing deformation.

The gradual incorporation of Cu into Al during HPT processing causes the local supersaturation of the metal matrix which ultimately induces the precipitation of Al_2Cu nanoparticles. These precipitates are already detected at the edge positions of the disc processed by one HPT turn, close to an interface of a Cu fragment. The nanoprecipitates are more abundant at later processing stages, especially after 30 HPT revolutions, and thereafter they coalesce into larger particles as follows from Figs 30, 31 and 32.

The formation of coherent Al_2Cu particles at *RT* would require several hours considering natural artificial ageing for Al-Cu alloys with similar compositions (ABBASCHIAN; ABBASCHIAN; REED-HILL, 2009). HPT processing therefore effectively accelerates the precipitation kinetics in the Al-4Cu alloy and this is probably due to the plentiful presence of high diffusivity paths such as grain boundaries and dislocations and the high density of vacancies within the Al-Cu solid solution. Additionally, the heat generated by straining leads to increases in the temperatures of the discs, estimated as ~327 and 330 K after 30 and 100 turns (EDALATI et al., 2018; FIGUEIREDO et al., 2012; PEREIRA et al., 2014), respectively, and these minor temperature rises may contribute to the fast ageing kinetics in the Al+4wt%Cu alloy.

The microstructural changes in the Al+4wt%Cu alloy during HPT prompt a gradual hardening with increasing numbers of revolutions. To visualise the effect of HPT processing by comparison with other Al-Cu alloys, the Vickers hardness and grain sizes achieved in this research and other investigations carried out using different SPD procedures are presented in Table 1 (ABD EL AAL, 2011; BRAGA et al., 2020; HAN et al., 2018; HUANG et al., 2012a, 2012b; JIA et al., 2018; LIU et al., 2010; MOHAMED et al., 2015; MURAYAMA; HORITA; HONO, 2001; XU et al., 2013).

Table 1: Grain size and Vickers hardness in Al-Cu alloys after SPD processing.

Material (wt%)	*Initial condition*	*SPD procedure*[a]	*Grain size (μm)*	*Vickers hardness (Hv)*	*References*
Al-4Cu	Cold-pressed powders	HPT: 6 GPa, 1 rpm, 1 turn[b]	~0.11	~160	This study
		HPT: 6 GPa, 1 rpm, 30 turns[b]	~0.06	~250	
		HPT: 6 GPa, 1 rpm, 100 turns[b]	~0.05	~270	
Al/Cu/Al	Stacked discs of Al/Cu/Al	HPT: 6 GPa, 1 rpm, 60 turns	~0.03	~500	(HAN et al., 2018)
Cu/Al/Cu	Stacked discs of Cu/Al/Cu	HPT: 5 GPa, 2 rpm, 5 turns	~0.1	~400	(DANILENKO et al., 2019)]
Al/Cu/Al	Stacked discs of Al/Cu/Al	HPT: 6 GPa, 1 rpm, 200 turns	~0.09	~435	(BAZARNIK et al., 2020)
Al/Cu/Al	Stacked discs of Al/Cu/Al	HPT: 6 GPa, 1 rpm, 10 turns	~0.25	~350	(KORZNIKOVA et al., 2020)
Al-4Cu	Solution treatment at 823 K for 5 h	HPT: 6 GPa, 1 rpm, 5 turns	~0.21	~200	(MOHAMED et al., 2015)
Al-4Cu	Solution treatment at 813 K for 2 h + ageing at 693 K for 2 h	HPT: 5 GPa, 1 rpm, 9 turns	~0.25	~150	(XU et al., 2013)
Al-5Cu	Solution treatment at 813 K for 24 h	ECAP: ϕ = 90°, route A, 4 passes	~0.70	~160	(JIA et al., 2018)
Al-4Cu	Annealing at 803 K for 3 h + slow cooling	ECAP: ϕ = 110°, route A, 8 passes	~0.70	~130	(BRAGA et al., 2020)
Al-4Cu	Solution treatment at 813 K for 1 h + ageing at 463 K for 16 h	ECAP: ϕ = 120°, route A, 6 passes	-	~105	(LIU et al., 2010)
Al-3.9Cu	Solution treatment at 793 K for 0.5 h	ECAP: ϕ = 90°, 8 passes	~0.10	~140	(MURAYAMA; HORITA; HONO, 2001)
	Solution treatment at 793 K for 0.5 h + ageing at 473 K for 26 h	ECAP: ϕ = 90°, 8 passes	~0.25	~100	
Al-3Cu	Homogenisation at 823 K for 7 days	ECAP: ϕ = 110°, route A, 8 passes	~0.11	~190	(ABD EL AAL, 2011)
Al-4Cu	Solution treatment at 813 K for 1 h + ageing at 463 K for 16 h	MDF: $\Delta\varepsilon$ = 0.4[c], 9 compressions	-	~100	(LIU et al., 2010)]
Al-4Cu	Solution treatment at 813 K for 2 h + ageing at 693 K for 2 h	MDF: $\Delta\varepsilon$ = 0.4[c], 35 compressions, 373 K[d]	~0.50	~100	(XU et al., 2013)
		MDF: $\Delta\varepsilon$ = 0.4[c], 9 compressions[d]	~0.80	~140	
Al-4Cu	Solution treatment at 813 K for 1 h + ageing at 463 K for 16 h	MDF: $\Delta\varepsilon$ = 0.4[c], 4 compressions	~0.25	~145	(HUANG et al., 2012a)
Al-4Cu	Solution treatment at 813 K for 1 h + ageing at 463 K for 16 h	MDF: $\Delta\varepsilon$ = 0.4[c], 12 compressions	~0.30	~105	(HUANG et al., 2012b)
		MDF: $\Delta\varepsilon$ = 0.4[c], 16 compressions	~0.20	~110	

[a] Processing conducted at *RT* if not otherwise mentioned.
[b] Disc radius of 4 mm.
[c] $\Delta\varepsilon$ refers to the amplitude of the imposed equivalent strain in each compression.
[d] Measurements undertaken after further annealing at 473 K for 1 h.

Examination of the results in Table 1 reveals that, in general, HPT processing promotes the generation of finer grain structures and a more substantial hardening in Al-Cu alloys than the application of MDF and ECAP. The strain imposed in each ECAP pass or MDF compression appears to play a role in the values of the Vickers hardness after processing. Higher hardness values are reached in material processed through ECAP dies with sharper internal channel angles and this may follow the higher strains imposed in each pass (IWAHASHI et al., 1996). Also, finer grain sizes are achieved in MDF procedures undertaken using larger strain amplitudes ($\Delta\varepsilon$) (FLAUSINO et al., 2019, 2020), and for all studies tabulated in Table 1 the MDF was performed with $\Delta\varepsilon \approx 0.4$ which gives lower strains in each pass by comparison with the reported results after ECAP.

After HPT, the microhardness gave values of >200 Hv but even higher values were achieved for stacked Al/Cu/Al discs processed by 60 turns (HAN et al., 2018; KAWASAKI et al., 2018). In this latter case, the synthesised nanocomposite reached a maximum hardness of ~500 Hv and exhibited a mean grain size of ~30 nm. For a given SPD procedure and Al-Cu alloys having lower Cu contents, there appears to exist a correlation between the initial condition and the steady state grain size. Higher hardness and smaller grain sizes are mostly achieved in alloys processed after the solution treatment, whilst materials processed in the aged and homogenised condition display less refined grains (MOHAMED et al., 2015; MURAYAMA; HORITA; HONO, 2001; XU et al., 2013).

To better understand the relationship between the material strength and the equivalent strain imposed in the Al+4wt%Cu alloy during HPT processing, the average values of the Vickers hardness recorded at the same radial position are plotted in Figure 34 as a function of the equivalent strains, ε_{HPT}. imposed on the discs. A thickness, *h,* of 0.7 mm was considered in the calculations using Valiev's equation (VALIEV et al., 1996). Additional datum points are included in Figure 34 for similar Al-Cu alloys subjected to SPD (ABD EL AAL, 2011; BRAGA et al., 2020; HUANG et al., 2012a, 2012b; JIA et al., 2018; LIU et al., 2010; MOHAMED et al., 2015; MURAYAMA; HORITA; HONO, 2001; XU et al., 2013).

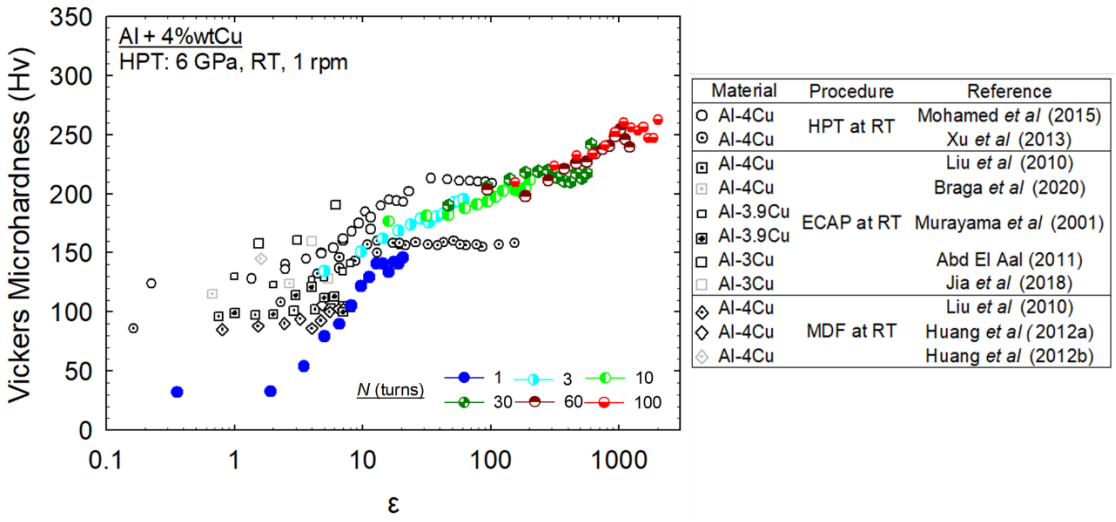

Figure 34: Plots of the Vickers microhardness as a function of equivalent strain (ε) for Al-Cu alloys with similar compositions subjected to various SPD procedures (ABD EL AAL, 2011; BRAGA et al., 2020; HUANG et al., 2012a, 2012b; JIA et al., 2018; LIU et al., 2010; MOHAMED et al., 2015; MURAYAMA; HORITA; HONO, 2001; XU et al., 2013).

The results shown in Figure 34 reveal that the Vickers hardness linearly increases with *log (ε)*, except for strains < 1 in which the material was not yet fully consolidated. Furthermore, HPT processing permits the achievement of higher strains than in MDF and ECAP and this consistently leads to the achievement of higher hardness values for alloys with similar compositions. It also follows from these plots that, in general, the materials having second-phase particles prior to SPD display lower Vickers hardness after processing.

In order to permit a clear visualisation of this phenomenon, the symbols associated with the data corresponding to this initial microstructural state are marked with internal points. Additionally, it is apparent that the saturation hardness in HPT processing related to the presence of a plateau in Fig.34 is achieved at lower strains in the Al-Cu alloy processed after ageing when compared with the same alloy processed by HPT after a solution treatment. This may be attributed to the higher Cu contents in the supersaturated Al-Cu alloy which in turn exhibits lower stacking fault energies and grain boundary mobilities

than the material with Cu partially in the form of second-phases (DOS SANTOS et al., 2023; HUANG; HUMPHREYS, 2012; HUMPHREYS; HATHERLY, 2004; SHIN et al., 2017).

The current results are consistent with these trends. First, at low strains, the microhardness values are lower than both the single and multiphasic materials. This originates from the lack of particle consolidation. After 3-10 turns, the Cu particles begin to fragment, causing the partial solubilisation of Cu into the Al matrix followed by the onset of nanoprecipitates and the refinement of the grain structures. This promotes a continuous hardening of the HPT-processed composite, surpassing the steady-state hardness attained in an Al-4Cu alloy processed by HPT after ageing at 693 K for 2 h (XU et al., 2013). Further deformation prompts a more intense fragmentation of Cu particles and it is not clear whether the material reaches an equilibrium condition at the edge of the discs after 100 HPT turns or whether additional strains are needed to reach equilibrium.

It is recognised that grain boundary strengthening in Al alloys may be modelled in terms of the Hall-Petch equation (FIGUEIREDO; KAWASAKI; LANGDON, 2023; HALL, 1951; PETCH, 1953) whereby the hardness (*H*) and the mean grain size ($\bar{L}$), as in earlier SPD studies (BAZARNIK et al., 2015; FURUKAWA et al., 1998; PEREIRA; HUANG; LANGDON, 2017), are given. Figure 35 displays a plot of Vickers microhardness as a function of $\bar{L}^{-1/2}$ for the Al+4wt%Cu alloy fabricated in this study and other alloys with similar compositions processed by MDF (HUANG et al., 2012a, 2012b; XU et al., 2013), ECAP (ABD EL AAL, 2011; BRAGA et al., 2020; MURAYAMA; HORITA; HONO, 2001) and HPT (MOHAMED et al., 2015; XU et al., 2013).

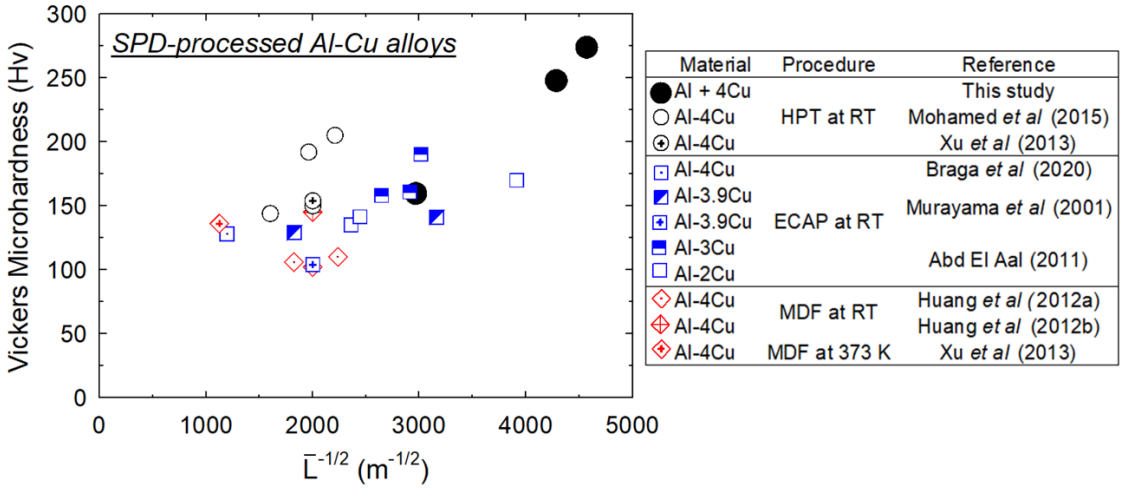

Figure 35: Plots of the Vickers microhardness as a function of $\bar{L}^{-1/2}$ for Al-Cu alloys with similar compositions processed by MDF (HUANG et al., 2012a, 2012b; XU et al., 2013), ECAP (ABD EL AAL, 2011; BRAGA et al., 2020; MURAYAMA; HORITA; HONO, 2001) and HPT (MOHAMED et al., 2015; XU et al., 2013).

Although the experimental datum points exhibit some scattering, the Vickers hardness increases with increasing values of $\bar{L}^{-1/2}$. Accordingly, superior hardening is achieved after HPT processing, followed by ECAP and MDF. The datum points corresponding to Al-Cu alloys with second phases before processing correspond to larger grain sizes and thus are on the left side of the Hall-Petch plot. It should be further noted that the Al+4wt%Cu composite synthesised in the present research consistently displays lower grains sizes and higher hardness than its counterparts processed from bulk alloys. Accordingly, this confirms the outstanding potential of using this fabrication route to consolidate metal powders with enhanced properties without relying on other processes that require high energies.

6 Conclusões

O presente trabalho discutiu a consolidação a frio de uma liga Al-4%Cu através de HPT. Os resultados apresentados e discutidos acima permitem as seguintes conclusões:

1- Um disco compactado a frio constituído a partir de uma mistura de pós de Al+4%wtCu foi processado por HPT para produzir um nanocompósito com granulometria de ~48 nm e microdureza Vickers máxima de ~270 Hv após 100 voltas.

2- Após uma volta de HPT, a liga Al-4Cu não estava totalmente consolidada devido à presença de microcavidades no centro do disco, o que levou a valores de dureza mais baixos neste local e desencadeou trincas precoces do metal durante a compressão em estado plano de deformação.

3- Uma consolidação completa, aliada a uma distribuição uniforme dos fragmentos de Cu ao longo das superfícies dos discos, foi obtida na liga processada em 30 voltas. Nesta fase, houve evidência para a dissolução parcial de Cu na matriz Al que exibiu um tamanho de grão de ~60 nm e uma distribuição abundante de precipitados Al2Cu coerentes com um diâmetro médio de ~2 nm.

4- Deformações adicionais de até 100 revoluções promoveram maior endurecimento, refinamento de grão e fragmentação dos domínios de Cu. No entanto, houve uma redução no número de frações dos precipitados concomitantemente com um aumento em seus tamanhos e perda de coerência com a solução sólida Al-Cu devido à coalescência das partículas.

6.1 Conclusions

The present work discussed the cold consolidation of an Al-4%Cu alloy through HPT. The results presented and discussed above enable the following conclusions:

1- A cold-pressed disc constituted by a mixture of Al+4%wtCu powders was processed by HPT to produce a nanocomposite with grain sizes of ~48 nm and a maximum Vickers microhardness of ~270 Hv after 100 turns.

2- After one HPT turn, the Al-4Cu alloy was not fully consolidated due to the presence of microcavities at the centre of the disc which led to lower hardness values at this location and triggered early metal cracking during plane strain compression.

3- A complete consolidation, coupled with a uniform distribution of Cu fragments throughout the surfaces of the discs, was achieved in the alloy processed through 30 turns. At this stage, there was evidence for the partial dissolution of Cu into the Al matrix which exhibited a grain size of ~60 nm and a plentiful distribution of coherent Al2Cu precipitates with an average diameter of ~2 nm.

4- Additional straining up to 100 revolutions promoted further hardening, grain refinement and fragmentation of Cu domains. Nevertheless, there was a reduction in the number fractions of precipitates concurrently with an increase in their sizes and loss of coherency with the Al-Cu solid solution due to particle coalescence.

8 References

ABBASCHIAN, R.; ABBASCHIAN, L.; REED-HILL, R. E. **Physical Metallurgy Principles**. Fourth ed. SI Version: Cengage Learning, 2009.

ABD EL AAL, M. I. Influence of the pre-homogenization treatment on the microstructure evolution and the mechanical properties of Al-Cu alloys processed by ECAP. **Materials Science and Engineering A**, v. 528, n. 22–23, p. 6946–6957, 25 ago. 2011.

ALMEIDA, N. G. S. et al. Mechanical behavior and microstructures of aluminum processed by low strain amplitude multi-directional confined forging. **Journal of Materials Research and Technology**, v. 9, n. 3, p. 3190–3197, 2020.

ALTAN, T.; NGAILE, G.; SHEN, G. (ED.). **Cold and hot forging: fundamentals and applications**. SI: ASM international, 2004. v. 1

ASGHARZADEH, H.; FARAGHI, H.; KIM, H. S. Fabrication of fullerene-reinforced aluminum matrix nanocomposites. **Acta Metallurgica Sinica (English Letters)**, v. 30, n. 10, p. 973–982, 1 out. 2017.

ASGHARZADEH, H.; JOO, S. H.; KIM, H. S. Consolidation of carbon nanotube reinforced aluminum matrix composites by high-pressure torsion. **Metallurgical and Materials Transactions A: Physical Metallurgy and Materials Science**, v. 45, n. 9, p. 4129–4137, 2014.

ASHIDA, M. et al. Production of Al/Al 2O 3 nanocomposites through consolidation by high-pressure torsion. **Materials Transactions**, v. 53, n. 1, p. 13–16, 2012.

AST, J.; DURST, K. Nanoforming behaviour and microstructural evolution during nanoimprinting of ultrafine-grained and nanocrystalline metals. **Materials Science and Engineering A**, v. 568, p. 68–75, 15 abr. 2013.

BACHMAIER, A. et al. The formation of supersaturated solid solutions in Fe-Cu alloys deformed by high-pressure torsion. **Acta Materialia**, v. 60, n. 3, p. 860–871, fev. 2012.

BACHMAIER, A. et al. New insights on the formation of supersaturated solid solutions in the Cu-Cr system deformed by high-pressure torsion. **Acta Materialia**, v. 69, p. 301–313, 2014.

BACHMAIER, A.; PIPPAN, R. **High-pressure torsion deformation induced phase transformations and formations: New material combinations and advanced properties**. **Materials Transactions**Japan Institute of Metals (JIM), , 2019.

BAZARNIK, P. et al. Structural impact on the Hall-Petch relationship in an Al-5Mg alloy processed by high-pressure torsion. **Materials Science and Engineering A**, v. 626, p. 9–15, 2015.

BAZARNIK, P. et al. Superior strength of tri-layered Al–Cu–Al nano-composites processed by high-pressure torsion. **Journal of Alloys and Compounds**, v. 846, p. 156380, abr. 2020.

BEYERLEIN, I. J.; TÓTH, L. S. **Texture evolution in equal-channel angular extrusion**. **Progress in Materials Science**, jun. 2009.

BEYGELZIMER, Y.; ORLOV, D.; VARYUKHIN', V. **A NEW SEVERE PLASTIC DEFORMATION METHOD: TWIST EXTRUSION**. , 2002.

BOUAZIZ, O.; KIM, H. S.; ESTRIN, Y. Architecturing of metal-based composites with concurrent nanostructuring: A new paradigm of materials design. **Advanced Engineering Materials**, v. 15, n. 5, p. 336–340, maio 2013.

BOYD, J. D.; NICHOLSON, R. B. **THE COARSENING BEHAVIOUR OF 0" AND 8' PRECIPITATES IN TWO Al-Cu ALLOYS**. , 1971.

BRAGA, D. P. et al. Microstructure, mechanical behavior and stress corrosion cracking susceptibility in ultrafine-grained Al-Cu alloy. **Materials Science and Engineering: A**, v. 773, p. 138865, 31 jan. 2020.

BRIDGMAN, P. **Studies in Large Plastic Flow and Fracture**. New York : McGraw-Hill, 1952.

BRIDGMAN, P. W. **Effects of High Shearing Stress Combined with High Hydrostatic Pressure**. , 1935. . Acesso em: 19 abr. 2023

BRIDGMAN, P. W. Shearing phenomena at high pressure of possible importance for geology. **THE JOURNAL OF GEOLOGY** , p. 653–669, 1936.

BRIDGMAN, P. W. Flow phenomena in heavily stressed metals. **Journal of Applied Physics**, v. 8, n. 5, p. 328–336, 1937.

BRUDER, E. **Formability of Ultrafine Grained Metals Produced by Severe Plastic Deformation–An Overview**. **Advanced Engineering Materials**Wiley-VCH Verlag, , 1 jan. 2019.

CARVALHO, A. P. et al. Using Plane Strain Compression Test to Evaluate the Mechanical Behavior of Magnesium Processed by HPT. **Metals**, v. 12, n. 1, 1 jan. 2022.

CASTRO, M. M. et al. Inverse Hall–Petch Behaviour in an AZ91 Alloy and in an AZ91–Al2O3 Composite Consolidated by High-Pressure Torsion. **Advanced Engineering Materials**, v. 22, n. 10, 1 out. 2020.

CHEN, Z.; ZHAO, Y.; ZHANG, Z. Theoretical and experimental study of precipitation and coarsening kinetics of θ′ phase in Al–Cu alloy. **Vacuum**, v. 189, 1 jul. 2021.

DANILENKO, V. N. et al. **Effect of annealing on the structure and phase composition of Al-Cu laminated metal-matrix composites produced by shear deformation under pressure**. IOP Conference Series: Materials Science and Engineering. **Anais**...Institute of Physics Publishing, 21 nov. 2018.

DANILENKO, V. N. et al. An approach for fabrication of Al-Cu composite by high pressure torsion. **Materials Letters**, v. 236, p. 51–55, abr. 2019.

DANILENKO, V. N. et al. Cu-Al metal matrix composite fabricated by accumulative HPT. **Materials Letters**, v. 300, 1 out. 2021.

DASHARATH, S. M.; MULA, S. Improvement of mechanical properties and fracture toughness of low SFE Cu-Al alloy through microstructural modification

by multiaxial cryoforging. **Materials Science and Engineering A**, v. 690, p. 393–404, 6 abr. 2017.

DOS SANTOS, I. C. et al. Evidence for two-stage hardening in an Al-Zn-Mg-Cu alloy processed by high-pressure torsion. **Journal of Alloys and Compounds**, v. 941, p. 10.1016, abr. 2023.

EDALATI, K. et al. Wear resistance and tribological features of pure aluminum and Al-Al2O3 composites consolidated by high-pressure torsion. **Wear**, v. 310, n. 1–2, p. 83–89, 15 fev. 2014.

EDALATI, K. et al. Effect of temperature rise on microstructural evolution during high-pressure torsion. **Materials Science and Engineering A**, v. 714, n. December 2017, p. 167–171, 31 jan. 2018.

EDALATI, K. et al. **Nanomaterials by severe plastic deformation: review of historical developments and recent advances**. **Materials Research Letters**Taylor and Francis Ltd., , 2022.

EDALATI, K.; HORITA, Z. **A review on high-pressure torsion (HPT) from 1935 to 1988**. **Materials Science and Engineering A**Elsevier Ltd, , 15 jan. 2016.

ETO, T.; SAT0, A.; MORF, T. STRESS-ORIENTED PRECIPITATION OF G.P. ZONES AND θ’ IN AN Al-Cu ALLOY. p. 499–508, 1978.

FIGUEIREDO, R. B. et al. Using finite element modeling to examine the temperature distribution in quasi-constrained high-pressure torsion. **Acta Materialia**, v. 60, n. 6–7, p. 3190–3198, 1 abr. 2012.

FIGUEIREDO, R. B.; CETLIN, P. R.; LANGDON, T. G. Using finite element modeling to examine the flow processes in quasi-constrained high-pressure torsion. **Materials Science and Engineering A**, v. 528, n. 28, p. 8198–8204, 2011.

FIGUEIREDO, R. B.; KAWASAKI, M.; LANGDON, T. G. Seventy years of Hall-Petch, ninety years of superplasticity and a generalized approach to the effect of grain size on flow stress. **Progress in Materials Science**, p. 101131, 20 abr. 2023.

FLAUSINO, P. C. A. et al. Microstructural evolution and mechanical behavior of copper processed by low strain amplitude multi-directional forging. **Materials Science & Engineering A**, v. 756, p. 474–483, 2019.

FLAUSINO, P. C. A. et al. Influence of Strain Amplitude on the Microstructural Evolution and Flow Properties of Copper Processed by Multidirectional Forging. **Advanced Engineering Materials**, v. 22, n. 4, p. 1901510, 2020.

FORD, H. Researches into the Deformation of Metals by Cold Rolling. **Proceedings of the Institution of Mechanical Engineers**, v. 159, n. 1, p. 115–143, jun. 1948.

FURUKAWA, M. et al. Factors influencing the flow and hardness of materials with ultrafine grain sizes. **Philosophical Magazine A**, v. 78, n. 1, p. 203–215, 1998.

GEIGER, M. et al. Microforming. **CIRP Annals - Manufacturing Technology**, v. 50, n. 2, p. 445–462, 2001.

GHALEHBANDI, S. M.; MALAKI, M.; GUPTA, M. **Accumulative roll bonding-A review**. **Applied Sciences (Switzerland)**MDPI AG, , 1 set. 2019.

GOODARZY, M. H. et al. The effects of room temperature ECAP and subsequent aging on mechanical properties of 2024 Al alloy. **Journal of Alloys and Compounds**, v. 585, p. 753–759, 2014.

HALL, E. O. The Deformation and Ageing of Mild Steel: III Discussion of Results. **Proceedings of the Physical Society**, v. Volume 64, n. 9, p. 747–753, 1951.

HALL, M. G.; HAWORTHJ, C. W. DISSOLUTION OF θ PHASE IN Al-5% Cu. p. 331–337, 1970.

HAN, J. K. et al. Direct Bonding of Aluminum–Copper Metals through High-Pressure Torsion Processing. **Advanced Engineering Materials**, v. 20, n. 11, 1 nov. 2018.

HAN, J. K. et al. **Bulk-state reactions and improving the mechanical properties of metals through high-pressure torsion**. **Materials Transactions**Japan Institute of Metals (JIM), , 2019.

HE, H. et al. Effects of deformation temperature on second-phase particles and mechanical properties of 2219 Al-Cu alloy. **Materials Science and Engineering A**, v. 712, p. 414–423, 17 jan. 2018.

HEWITT, P.; BUTLER, E. P. MECHANISMS AND KINETICS OF θ' DISSOLUTION IN Al-3% Cu. **Acra metail**, v. 34, n. 7, p. 1163, 1986.

HORITA, Z.; EDALATI, K. Severe plastic deformation for nanostructure controls. **Materials Transactions**, v. 61, n. 11, p. 2241–2247, 18 set. 2020.

HORNBOGEN, E. Hundred years of precipitation hardening. **Journal of Light Metals**, v. 1, p. 127–132, 2001.

HUANG, W. et al. Reprecipitation behavior in Al-Cu binary alloy after severe plastic deformation-induced dissolution of θ' particles. **Materials Science and Engineering A**, v. 546, p. 26–33, 1 jun. 2012a.

HUANG, W. et al. Severe plastic deformation-induced dissolution of θ" particles in Al-Cu binary alloy and subsequent nature aging behavior. **Materials Science and Engineering A**, v. 556, p. 801–806, 30 out. 2012b.

HUANG, Y. et al. The fabrication of graphene-reinforced Al-based nanocomposites using high-pressure torsion. **Acta Materialia**, v. 164, p. 499–511, 1 fev. 2019.

HUANG, Y.; HUMPHREYS, F. J. The effect of solutes on grain boundary mobility during recrystallization and grain growth in some single-phase aluminium alloys. **Materials Chemistry and Physics**, v. 132, n. 1, p. 166–174, 16 jan. 2012.

HUANG, Y.; KAWASAKI, M.; LANGDON, T. G. Influence of Anvil Alignment on Shearing Patterns in High-Pressure Torsion. **Advanced Engineering Materials**, v. 15, n. 8, p. 747–755, 1 ago. 2013.

HUMPHREYS, F. J.; HATHERLY, M. **Recrystallization and Related Annealing Phenomena, Second edition**. Oxford: Pergamon Press, 2004.

I J POLMEAR. Aluminium Alloys-A Century of Age Hardening. **MATERIALS FORUM**, v. 28, 2004.

IMAYEV, R. M.; IMAYEV, V. M.; SALISHCHEV, G. A. Formation of submicrocrystalline structure in TiAI intermetallic compound. p. 4465–4471, 1992.

IWAHASHI, Y. et al. Principle of equal-channel angular pressing for the processing of ultra-fine grained materials. **Scripta Materialia**, v. 35, n. 2, p. 143–146, 1996.

JIA, H. et al. Quantifying the grain boundary segregation strengthening induced by post-ECAP aging in an Al-5Cu alloy. **Acta Materialia**, v. 155, p. 199–213, 15 ago. 2018.

JIANG, W. et al. On the Heterogeneity of Local Shear Strain Induced by High-Pressure Torsion. **Advanced Engineering Materials**, v. 22, n. 1, p. 1900477, 1 jan. 2020.

JOO, S. H.; KIM, H. S. Ring-Constraint High-Pressure Torsion Process. **Metallurgical and Materials Transactions A: Physical Metallurgy and Materials Science**, v. 47, n. 7, p. 3473–3478, 1 jul. 2016.

KAWASAKI, M. et al. Fabrication of nanocomposites through diffusion bonding under high-pressure torsion. **Journal of Materials Research**, v. 33, n. 18, p. 2700–2710, 2018.

KAWASAKI, M.; LANGDON, T. G. The significance of strain reversals during processing by high-pressure torsion. **Materials Science and Engineering A**, v. 498, n. 1–2, p. 341–348, 20 dez. 2008.

KAWASAKI, M.; LANGDON, T. G. **Review: Achieving superplasticity in metals processed by high-pressure torsion**. Journal of Materials Science. **Anais**...Kluwer Academic Publishers, 2014.

KAWASAKI, M.; LANGDON, T. G. **Review: achieving superplastic properties in ultrafine-grained materials at high temperatures**. **Journal of Materials Science**Springer New York LLC, , 20 jun. 2015.

KHAJOUEI-NEZHAD, M. et al. Microstructure and mechanical properties of ultrafine-grained aluminum consolidated by high-pressure torsion. **Materials Science and Engineering A**, v. 682, p. 501–508, 13 jan. 2017.

KHISAMOV, R. K. et al. Microstructure, microhardness and work function of in-situ Al-Cu composite processed by mechanical alloying by means of high-pressure torsion. **Continuum Mechanics and Thermodynamics**, 2022.

KOCICH, R.; KUNICKÁ, L.; MACHÁKOVÁ, A. **Twist Channel Multi-Angular Pressing (TCMAP) as a method for increasing the efficiency of SPD**. IOP Conference Series: Materials Science and Engineering. **Anais**...Institute of Physics Publishing, 2014.

KORMOUT, K. S.; PIPPAN, R.; BACHMAIER, A. **Deformation-Induced Supersaturation in Immiscible Material Systems during High-Pressure Torsion**. **Advanced Engineering Materials**Wiley-VCH Verlag, , 1 abr. 2017.

KORZNIKOV, A. V et al. INFLUENCE OF SEVERE PLASTIC DEFORMATION ON STRUCTURE AND PHASE COMPOSITION OF CARBON STEEL. **Pergamon NanoStructured Materials**, v. 4, n. 2, p. 159–167, 1994.

KORZNIKOVA, G. et al. Influence of Constrained High-Pressure Torsion on Microstructure and Mechanical Properties of an Aluminum-Based Metal Matrix Composite. **JOM**, v. 72, n. 8, p. 2898–2911, 1 ago. 2020.

KULAGIN, R. et al. Modelling of High Pressure Torsion using FEM. **Procedia Engineering**, v. 207, p. 1445–1450, abr. 2017.

KULAGIN, R. et al. Instabilities of interfaces between dissimilar metals induced by high pressure torsion. **Materials Letters**, v. 222, p. 172–175, 1 jul. 2018.

LAIRDT, C.; AARONSON, H. I. MECHANISMS OF FORMATION OF θ AND DISSOLUTION OF θ’ PRECIPITATES IN AN Al-d% Cu ALLOY. p. 171–185, 1966.

LANGDON, T. G. **Seventy-five years of superplasticity: Historic developments and new opportunities**. **Journal of Materials Science**, nov. 2009.

LANGDON, T. G. Achieving superplasticity in ultrafine-grained metals. **Mechanics of Materials**, v. 67, p. 2–8, 2013.

LIU, Z. et al. The dissolution behavior of θ’ phase in Al-Cu binary alloy during equal channel angular pressing and multi-axial compression. **Materials Science and Engineering A**, v. 527, n. 16–17, p. 4300–4305, jun. 2010.

LIU, Z. et al. On strain-induced dissolution of θ′ and θ particles in Al-Cu binary alloy during equal channel angular pressing. **Materials Science and Engineering A**, v. 528, n. 6, p. 2217–2222, 15 mar. 2011.

LUBARDA, V. A. On the effective lattice parameter of binary alloys. **Mechanics of Materials**, v. 35, n. 1–2, p. 53–68, 1 jan. 2003.

LUGO, N. et al. Microstructures and mechanical properties of pure copper deformed severely by equal-channel angular pressing and high pressure torsion. **Materials Science and Engineering A**, v. 477, n. 1–2, p. 366–371, 25 mar. 2008.

LUTTEROTTI, L.; SCARDI, P. Simultaneous structure and size-strain refinement by the rietveld method. **Journal of Applied Crystallography**, v. 23, p. 246–252, 1990.

MACHADO, D. C. et al. Influence of processing temperature on microhardness evolution, microstructure and superplastic behaviour in an Al–Mg alloy processed by high-pressure torsion. **Journal of Materials Research and Technology**, v. 24, p. 2850–2867, abr. 2023.

MANJUNATH, G. A. et al. **A review on effect of multi-directional forging/multi-axial forging on mechanical and microstructural properties of aluminum alloy**. Materials Today: Proceedings. **Anais**...Elsevier Ltd, 2021.

MASSALSKI, T. B. **The Al-Cu (Aluminum-Copper) System Al-Cu**. Pittsburg: Bulletin of Alloy Phase Diagrams, 1980. v. 1

MAZILKIN, A. et al. **Phase transformations induced by severe plastic deformation**. **Materials Transactions**Japan Institute of Metals (JIM), , 2019.

MERICA, P. D. ALUMINUM AND ITS LIGHT ALLOYS. p. 350–353, 1920.

MOHAMED, I. F. et al. Age hardening and thermal stability of Al-Cu alloy processed by high-pressure torsion. **Materials Science and Engineering A**, v. 627, p. 111–118, 1 mar. 2015.

MOHAMMADI, A. et al. Developing age-hardenable Al-Zr alloy by ultra-severe plastic deformation: Significance of supersaturation, segregation and precipitation on hardening and electrical conductivity. **Acta Materialia**, v. 203, 15 jan. 2021.

MOLINA-OCAMPO, A. et al. Optimized synthesis of a nanostructured Al alloy modified with Cu by mechanical alloying-Microstructureand solubility modelling perspective. **CITATION 1 READS 263 Digest Journal of Nanomaterials and Biostructures**, v. 11, n. 2, 2016.

MURAYAMA, M.; HORITA, Z.; HONO, K. Microstructure of two-phase Al-1.7 at% Cu alloy deformed by equal-channel angular pressing. **Acta mater**, v. 49, p. 21–29, 2001.

NASEDKINA, Y. et al. Mechanisms of precipitation induced by large strains in the Al-Cu system. **Journal of Alloys and Compounds**, v. 710, p. 736–747, 2017.

NING, J. L.; WANG, D. Concurrent high strength and high ductility in isotropic bulk Cu-Al alloy with three-dimensional nano-twinned structure. **Journal of Alloys and Compounds**, v. 514, p. 214–219, 15 fev. 2012.

NISHIDA, Y. et al. Rotary-die equal-channel angular pressing of an Al-7 mass% Si-0.35 mass% Mg alloy. p. 261–266, 2001.

NUTTING, J. Some aspects of structure-property relationship in materials. Em: UNIVERSITY OF CALIFORNIA PRESS (Ed.). **Electron Microscopy and Structure of Materials**. Berkeley, CA, USA: [s.n.]. p. 617–636.

OH-ISHI, K. et al. High-pressure torsion for enhanced atomic diffusion and promoting solid-state reactions in the aluminum–copper system. **Acta Materialia**, v. 61, n. 9, p. 3482–3489, abr. 2013.

PARIMI, A. K.; ROBI, P. S.; DWIVEDY, S. K. Severe plastic deformation of copper and Al-Cu alloy using multiple channel-die compression. **Materials and Design**, v. 32, n. 4, p. 1948–1956, abr. 2011.

PATIL, D. C. et al. **Using ball indentation to determine the mechanical properties of an Al-7475 alloy processed by high-pressure torsion**. Journal of Materials Science. **Anais**...jul. 2013.

PEREIRA, P. H. R. et al. Modeling the temperature rise in high-pressure torsion. **Materials Science and Engineering A**, v. 593, p. 185–188, abr. 2014.

PEREIRA, P. H. R.; FIGUEIREDO, R. B. Finite element modelling of high-pressure torsion: An overview. **Materials Transactions**, v. 60, n. 7, p. 1139–1150, 2019.

PEREIRA, P. H. R.; HUANG, Y.; LANGDON, T. G. Examining the microhardness evolution and thermal stability of an Al–Mg–Sc alloy processed by high-pressure torsion at a high temperature. **Journal of Materials Research and Technology**, v. 6, n. 4, p. 348–354, 2017.

PETCH, N. J. The Cleavage Strength of Polycristals. **Journal of The Iron And Steel Institute**, p. 25–28, 1953.

PIPPAN, R. et al. **Advantages and limitations of HPT: A review**. Materials Science Forum. **Anais**...Trans Tech Publications Ltd, 2008.

RADHI, H. N.; ALJASSANI, A. M. H.; MOHAMMED, M. T. **Effect of ECAP on microstructure, mechanical and tribological properties of aluminum and brass alloys: A review**. Materials Today: Proceedings. **Anais**...Elsevier Ltd, 2019.

RIETVELD, H. M. A profile refinement method for nuclear and magnetic structures. **Journal of Applied Crystallography**, v. 2, n. 2, p. 65–71, 1969.

SAITO, Y. et al. ULTRA-FINE GRAINED BULK ALUMINUM PRODUCED BY ACCUMULATIVE ROLL-BONDING (ARB) PROCESS. 1998.

SAUVAGE, X.; DUCHAUSSOY, A.; ZAHER, G. **Strain induced segregations in severely deformed materials**. **Materials Transactions**Japan Institute of Metals (JIM), , 2019.

SEGAL, V. **Review: Modes and processes of severe plastic deformation (SPD)**. **Materials**MDPI AG, , 10 jul. 2018.

SEGAL, V. M. **Methods of Stress-Strain Analyses in Metal Forming**. Minsk, Russia: [s.n.].

SEGAL, V. M. **A Materials processing by simple shear**. [s.l: s.n.].

SHIN, D. et al. Solute segregation at the Al/θ′-Al2Cu interface in Al-Cu alloys. **Acta Materialia**, v. 141, p. 327–340, 1 dez. 2017.

SILVA, C. et al. Interface structures in Al-Nb2O5 nanocomposites processed by high-pressure torsion at room temperature. **Materials Characterization**, v. 162, 1 abr. 2020.

SILVA, P. H. et al. Strain partitioning in a dual-phase steel under plane strain compression. **Materials Science and Engineering A**, v. 862, 18 jan. 2023.

STEMLER, P. M. A. et al. Mechanical behavior and microstructures of aluminum in the Multi-Axial Compression (MAC) with and without specimen re-machining. **Materials Letters**, v. 237, p. 84–87, 15 fev. 2019.

TASAN, C. C. et al. Integrated experimental-simulation analysis of stress and strain partitioning in multiphase alloys. **Acta Materialia**, v. 81, p. 386–400, 2014.

TOKUNAGA, T. et al. Microstructure and mechanical properties of aluminum-fullerene composite fabricated by high pressure torsion. **Scripta Materialia**, v. 58, n. 9, p. 735–738, maio 2008.

TOKUNAGA, T.; KANEKO, K.; HORITA, Z. Production of aluminum-matrix carbon nanotube composite using high pressure torsion. **Materials Science and Engineering A**, v. 490, n. 1–2, p. 300–304, 25 ago. 2008.

TSUJI, N. et al. ARB (accumulative roll-bonding) and other new techniques to produce bulk ultrafine grained materials. **Advanced Engineering Materials**, v. 5, n. 5, p. 338–344, 1 maio 2003.

VALIEV, R. Z. et al. Structure and deformaton behaviour of Armco iron subjected to severe plastic deformation. **Acta Materialia**, v. 44, n. 12, p. 4705–4712, 1996.

VALIEV, R. Z. et al. On the origin of the extremely high strength of ultrafine-grained Al alloys produced by severe plastic deformation. **Scripta Materialia**, v. 63, n. 9, p. 949–952, 2010.

VALIEV, R. Z.; ISLAMGALIEV, R. K.; ALEXANDROV, I. V. Bulk nanostructured materials from severe plastic deformation. p. 103–189, 2000.

VALIEV, R. Z.; ISLAMGALIEV, R. K.; SEMENOVA, I. P. Superplasticity in nanostructured materials: New challenges. **Materials Science and Engineering A**, v. 463, n. 1–2, p. 2–7, 15 ago. 2007.

VALIEV, R. Z.; ISLAMGALIEV, R. K.; YUNUSOVA, N. F. **Grain refinement and enhanced superplasticity in metallic materials**. Materials Science Forum. **Anais**...Trans Tech Publications Ltd, 2001.

VALIEV, R. Z.; LANGDON, T. G. **Principles of equal-channel angular pressing as a processing tool for grain refinement**. **Progress in Materials Science**, set. 2006.

VALIEV, R. Z.; LANGDON, T. G. **The art and science of tailoring materials by nanostructuring for advanced properties using SPD techniques**. **Advanced Engineering Materials**, ago. 2010.

VOLLERTSEN, F. et al. State of the art in micro forming and investigations into micro deep drawing. **Journal of Materials Processing Technology**, v. 151, n. 1- 3 SPEC. ISS., p. 70–79, 1 set. 2004.

VOLLERTSEN, F.; SCHULZE NIEHOFF, H.; HU, Z. State of the art in micro forming. **International Journal of Machine Tools and Manufacture**, v. 46, n. 11 SPEC. ISS., p. 1172–1179, 2006.

WAN, B. et al. **Review of solid state recycling of aluminum chips**. **Resources, Conservation and Recycling**Elsevier B.V., , 2017.

WILM, A. DRP 244554 (German patent). **Metallurgie**, v. 8, p. 233, 1906.

WILM, A. Physikalisch-metallurgische Untersuchungen über magnesiumhaltige Aluminiumlegierungen. **Metallurgie: Zeitschrift für de gesamte Hüttenkunde**, v. 8, n. 8, p. 225–227, 1911.

XU, X. et al. Using an Al-Cu binary alloy to compare processing by multi-axial compression and high-pressure torsion. **Materials Science and Engineering A**, v. 588, p. 280–287, 20 dez. 2013.

ZENER, C.; HOLLOMON, J. H. Effect of strain rate upon plastic flow of steel. **Journal of Applied Physics**, v. 15, n. 1, p. 22–32, 1944.

ZHANG, F. et al. Fast hydrolysis and hydrogen generation on Al-Bi alloys and Al-Bi-C composites synthesized by high-pressure torsion. **International Journal of Hydrogen Energy**, v. 42, n. 49, p. 29121–29130, 7 dez. 2017.

ZHANG, Y. et al. Strengthening mechanisms in an ultrafine-grained Al-Zn-Mg-Cu alloy processed by high pressure torsion at different temperatures. **Materials Science and Engineering: A**, v. 752, p. 223–232, 2019a.

ZHANG, Y. et al. Dynamic precipitation, segregation and strengthening of an Al-Zn-Mg-Cu alloy (AA7075) processed by high-pressure torsion. **Acta Materialia**, v. 162, p. 19–32, 2019b.

ZHAO, L.; LU, H.; GAO, Z. Microstructure and Mechanical Properties of Al/Graphene Composite Produced by High-Pressure Torsion. **Advanced Engineering Materials**, v. 17, n. 7, p. 976–981, 1 jul. 2015.

ZHILYAEV, A. P. et al. Particle and grain growth in an Al-Si alloy during high-pressure torsion. **Scripta Materialia**, v. 57, n. 8, p. 763–765, out. 2007.